Hotspot Endurance Testing of Thin Amorphous Silicon Solar Foils

The importance of reliability

Peer Sluijs

Delft University of Technology

TU Delft

Hotspot Endurance Testing of Thin Amorphous Silicon Solar Foils

The importance of reliability

by

Peer Sluijs

to obtain the degree of Master of Science
at the Delft University of Technology,
to be defended publicly on Tuesday September 26, 2023 at 15:00.

Student number:	4957660	
Project duration:	January – September 2023	
Thesis committee:	Prof. Dr. Ir. A. H. M. Smets,	TU Delft, Supervisor (PVMD)
	Dr. H. Ziar,	TU Delft (PVMD)
	Dr. Ir. A. Shekhar,	TU Delft (DCES)
	Dr. S. K. Pullayikody,	TU Delft, Daily supervisor (PVMD)

This thesis is confidential and cannot be made public until December 31, 2024.

TU Delft

Preface

This thesis report is written for my Master of Science in Sustainable Energy Technology (SET) at the Delft University of Technology. In the last nine months, I have been researching the hotspot reliability of thin amorphous silicon foils as part of a larger research on thin-film PV technologies in the Photovoltaic Material and Devices (PVMD) group and in close ties with the company HyET Solar.

While writing this report, I assumed that the reader has basic knowledge of solar modules and how they work. Those unfamiliar with the IEC standards for solar modules or those who wish to revise their knowledge can read Chapter 2. Readers who are interested in the methodology can read Chapter 3 and the ones who are curious about the results, can read Chapters 4 to 6.

First off, I would like to give my heartfelt thanks to my daily supervisor Sreejith Koorthedath Pullayikody for being my daily supervisor and being there every step of the way during my thesis, but also for his insights and discussions. I would like to thank Ravi Vasudevan, Gayathri Mathiazhagan and the other people at HyET for letting us use their facilities for our experiments, as well as for their insights during the Flamingo Meetings. Next, I want to give a huge thanks to Arno Smets for his guidance and insights and most of all, for recommending this thesis topic to me. Finally, I want to thank my parents and friends for always supporting me and having my back.

Peer Sluijs
Delft, September 2023

Abstract

Thin-film amorphous Silicon (a-Si) technology has been up and coming in recent years in order to achieve an efficiency comparable to crystalline Silicon (c-Si). Although the technology has existed for quite some time, it has not been researched as much as its crystalline counterpart, especially not in the hotspot reliability sector. The hotspot phenomenon is noticed in field-aged modules commonly due to partial shading or soiling losses. When one of the cells in a string gets partially or fully shaded, the shaded cells are forced to be in reverse bias and dissipate power in the form of heat, causing the formation of hotspots. The hotspots can reach temperatures of beyond 100°C. These can lead to the melting of module encapsulants and faster degradation of the module, as well as being a fire hazard because of the elevated temperatures. This thesis was done in collaboration with HyET Solar BV, a company that produces a-Si thin film solar foils. The modules used in this thesis are from HyET Solar BV and we have selected highly degraded modules for the experiments.

This report aims to achieve a couple of things: first, get insight of hotspot formation in a-Si thin-film modules in accordance with the latest *International Electrotechnical Comission* (IEC) 61215 Certification norms.

Secondly, we have utilized electroluminescence (EL) imaging to classify various defects present in the modules and to evaluate their endurance to hotspot formation. Based on those results, we created a map that shows the probability of hotspot formation from different defects in the degraded modules.

And lastly, we classified the different kinds of hotspots based on factors like shape and location. Also, the possibilities of how these defects originated are explained on the basis of a schematic overview of the interconnection between the cells.

After testing and experimenting, it became apparent that the highly degraded a-Si foils are susceptible to hotspot formation. After light soaking two foils according to the IEC 61215 norms, a couple of hotspots were created in the shaded area. Some of these hotspots could be seen on EL images by defects before they became visible during the visual inspection step. EL imaging is used to characterize different defects that could lead to hotspot formation. These defects are white dots, current crowding and dark regions. The probability map for these defects is as follows: 46.6% of the white dots have turned into hotspots, 16.7% for current crowding and 32% for dark regions. It is suspected that these white dots are a manufacturing process problem; they could be areas of high-impurity contaminants or a sharp point. Current crowding and dark regions are always paired together and depending on which side of the cell they are on, it is suspected that it is a fault in either the P2 or P3 scribes of a cell in the module.

It is our recommendation to investigate the interconnection between the cells, with a focus on the scribes, as these might be the culprits for the current crowding and dark region defects. Also, different settings and a different lens might be used to create different EL images that might show defects or other things that were not visible in the EL images created during this thesis. The reverse bias characteristics of each cell are also recommended to be investigated to see any correlation with hotspot formation, as well as the role of aging of modules. Lastly, the analysis should also be done on no degraded or new modules and on modules with different sizes and dimensions to see if that shows different results.

Contents

List of Figures

Nomenclature

Abbreviations

Abbreviation	Definition
a-Si	Amorphous Silicon
c-Si	Crystalline Silicon
EL	Electroluminescence
IEC	International Electrotechnical Commission
IR	Infrared
LASS	Large Area Solar Simulator
LS	Light Soaking
OC	Open-circuit
PV	Photovoltaic
SC	Short-circuit
WCSS	Worst Case Shadowing Scenario

Symbols

Symbol	Definition	Unit
E	Energy	[eV]
FF	Fill Factor	[%]
I	Current	[A]
$I(^*)$	Current Range	[A]
I_{MP}	Maximum Power Current	[A]
I_{SC}	Short-circuit Current	[A]
I	Irradiance	[W/m^2]
P	Power	[W]
P_{max}	Maximum Power	[W]
P_{min}	Minimum Power	[W]
T	Temperature	[$^\circ$C]
V	Voltage	[V]
V_{OC}	Open-circuit Voltage	[V]

1

Introduction

Significant efforts have been made in the Solar Photovoltaic (PV) sector in recent years to support the Net Zero Scenario by 2050. The PV generation have increased by 26% in 2022 [1]. While it is now on track to achieve this scenario, maintaining the generation growth requires reaching annual capacity additions nearly three times higher than in 2022 until 2030 [1]. Besides the greater policy ambition and more effort from both private and public stakeholders, additional research and development in the technology are also needed to create more efficient and reliable solar panels. Crystalline silicon (c-Si) continues to be the dominant technology for PV modules, with a market share of over 95% [2]. One of the upcoming technologies is thin film amorphous silicon (a-Si). Although it has a lower efficiency compared to c-Si, it does have several advantages, like lower costs, flexibility, better low-light performance on overcast days and better temperature coefficient [3]. However, more research is needed, particularly on the reliability of thin-film a-Si solar panels and the various degradation mechanisms associated with them. Very little literature is available on hotspot formation in thin-film a-Si solar modules in this context.

The aim of this thesis is to gain insights into a deeper understanding of hotspot formation in thin-film a-Si modules. Several advanced characterization techniques were used, such as the Large Area Solar Simulator (LASS), an electroluminescence (EL) camera and a light soaking machine in order to reach these insights. Also, facilities from Hyet Solar BV have been used in close collaboration, to ensure that the hotspot testing is done on industrially designed solar foils.

The thesis is constructed as follows. Chapter 2 will discuss the background study, the literature review on hotspot formation and the steps involved in the testing of hotspot as per the latest International Electrotechnical Commission (IEC) 61215 procedure. Then, Chapter 3 describes the methodology, different characterization methods and different light soaking machinery used in this thesis. Next, Chapters 4 to 6 are all results chapters; Chapter 4 discusses the results of hotspot formation in thin-film a-Si modules when subjected to hotspot endurance testing according to the IEC 61215 certification norms. Chapter 5 explains various defect types observed in a-Si modules and the probability map of defects turning into hotspots. Chapter 6 classifies hotspots and provides insights into the shape, location and cause of these hotspots. The last chapter offers a conclusion of this work and summarizes the future scope of this work.

2

Background Study

This chapter deals with the knowledge and theory needed to understand how this research is conducted. Firstly, the importance of reliability and the IEC standards will be discussed. After that, the origins of hotspots, the need and importance of testing will be explained. Further, the steps of the hotspot IEC 61215 Certifcation norms will be explained. Finally, this chapter provides a brief literature review of hotspot formation in crystalline and a-Si modules.

2.1. Reliability and IEC Standards

The solar modules employed in the field should ensure that they provide an up-to-quality energy yield for a guaranteed lifetime. Manufacturers provide two warranties: product warranty and performance warranty. While product warranty may vary between 10-20 years depending on the type of module, performance warranty is typically for 25 years. This is to ensure a certain level of energy output throughout its lifetime [4]. In order for solar module manufacturers to guarantee their consumers reliable products, these modules have to uphold a certain standard. To ensure these standards, the modules have to undergo and pass accelerated tests imposed by the IEC. The IEC is a non-profit organization leading the world in the preparation and publication of international standards for all electrical, electronic and related technologies.

The standard which is about the requirements for the qualification process and type and design approval of terrestrial PV modules suitable for long-term operation in general open-air climates, is described in the latest IEC 61215 certification norms [5]. Its main purpose is to ensure the reliability of the modules and to raise the quality standards of PV manufacturing. The solar modules are tested for all failures that can occur during the field operation. It also guarantees the quality inspection of the modules for different criteria that can not be perceived by visual inspection. There are 19 module quality tests performed under the IEC 61215 certification, which are done at accelerated conditions in order to mimic the 25-year lifetime of a solar module and measure mechanical, environmental, performance and safety aspects. Few of the major accelerated tests are:

- **Insulation test**: Determines whether or not the module is sufficiently insulated between current-carrying parts and the frame or the outside world.
- **Outdoor exposure test**: Assesses the ability of the module to tolerate exposure to outdoor conditions and also to unveil any degradation effects.
- **Ultra Violet (UV) preconditioning test**: Looks to identify materials and adhesive bonds that are susceptible to UV degradation.
- **Thermal cycling test**: Looks at the ability of the module to withstand fatigue, thermal mismatches and other stresses caused by temperature change.
- **Humidity-freeze test**: Checks the ability of the module to withstand the effects of high temperature and humidity followed by sub-zero temperatures.
- **Damp-heat test**: Determines the ability of the module to resist the effects of long-term penetration of humidity.
- **Hail test**: Checks if the module is able to resist the impact of hailstones.

In order for the solar modules to be approved for commercialization, they have to pass all the tests. To pass the tests, the degradation should not be more than around 5% after each test, as well as no indication of any visual defects.

2.2. Hotspot endurance testing

2.2.1. Origins and importance of hotspots

A hotspot is an area in a solar cell in which the temperature is much higher than the surrounding area. As shown in Figure 2.1, when one of the cells in a series connected string gets shadowed, the overall current becomes limited by this shadowed cell if the operating current of the string approaches the I_{SC} of this cell.

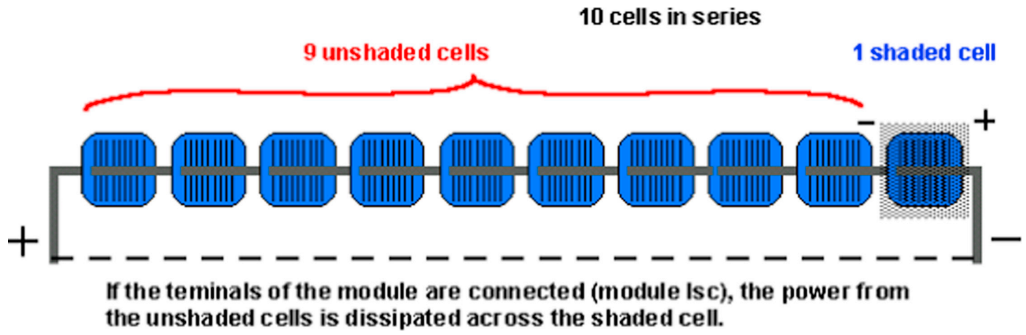

Figure 2.1: String of series connected cells in which one cell is shaded, which can lead to the creation of hotspots [6].

The unshadowed cells force the shadowed cell to go into reverse bias. The excessive power in the shadowed cell is dissipated in the form of heat, causing local overheating, the hotspots, which can have temperatures up to 150°C [7]. These temperatures can have detrimental effects, such as cell/glass cracking and melting of solder, which leads to the degradation of the solar cell, as can be seen in Figure 2.2. On top of that, it is a fire hazard, as the high temperatures can cause fire outbreaks.

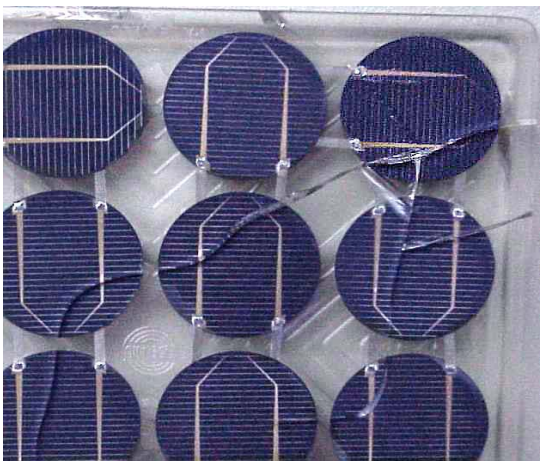

(a) Cracked cell [8]

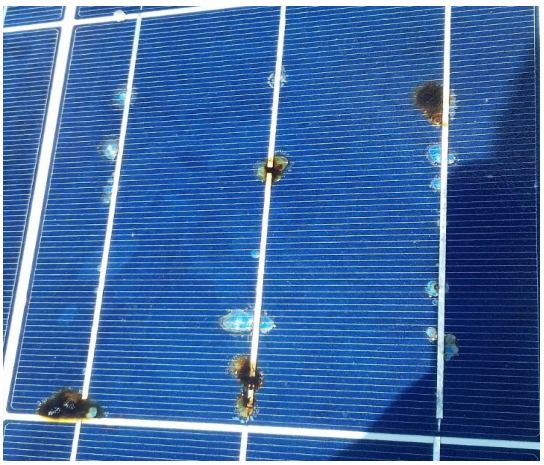

(b) Hotspots [9]

Figure 2.2: Failures as a result of high temperatures because of a shaded cell

2.2.2. IEC 61215 certification procedure

It is important to test solar modules for their susceptibility to form hotspots, as hotspots not only affect the performance but also is a safety concern in the field. For this thesis, only modules with a series connection of cells in a single string are reported. Hence, the IEC 61215 standard procedure for series-connected cells is only presented in this section. For the procedure, the following machinery/apparatus are used:

- **Radiant source**
- **I-V curve tracer**
- **Opaque covers to shadow the cells**
- **Temperature detector**

For the hotspot endurance test, these steps have to be followed according to the IEC 61215 certification guideline in order to determine the worst case shadowing scenario (WCSS):

1. The module, un-shadowed, has to get exposed to a radiant source providing a total irradiance of 800 - 1100 W/m^2 at the module surface. The following sources can be used:
   (a) A pulsed simulator in which the temperature of the module will be near room temperature (25 $\pm$ 5)°C.
   (b) A steady-state simulator where the temperature of the module shall be maintained within $\pm$5°C before beginning with the measurements.
   (c) Sunlight where the temperature of the module shall be maintained within $\pm$5°C before beginning with the measurements.
2. After the module is thermally stable, measure the I-V characteristic of the module and determine the maximum power current I_{MP1} and maximum power P_{max1}. Determine the range of the maximum power current (I_{min} < I < I_{max}). Here, I_{min} is 0.95I_{max} and I_{max} is the maximum power current of the un-shadowed module. This current range is named $I(^*)$.
3. Measure the I_{SC} at each position described in step 4.
4. Starting from one side of the module, use an opaque cover to completely obscure one cell. Gradually slide the cover along the cells and increase the number of shadowed cells until the I_{SC} falls within the current range of the non-shadowed module. Under these circumstances, the maximum power is dissipated within the shadowed group of cells. Between I_{SC} measurements, the maximum increment is equal to one cell width. The minimum shaded area is two cell widths. If achieving the current within the specified range requires shadowing fewer than two cells, then the shaded area shall be fixed at the minimum. When shadowing for some number of "x" cells results in a current that is too high, and if shadowing x+1 cells results in a current that is too low, then the narrower shadowed area (x cells) must be opted for.
5. Slide the opaque cover, with the dimensions found in the previous step, across the module and at each position, measure the I_{SC}. The biggest step size between measurements is the width of the shadowed area, which means that each cell shall be shaded at some point. If the I_{SC} falls below $I(^*)$, reduce the width of the cover with increments of one cell width until the current is within the range again. If the scenario occurs in which the shadowed area is reduced to the minimum of two cell widths, it shall not be reduced further. Furthermore, the irradiance shall not change by more than $\pm$2% during the process. For the remaining steps, the shadowed area is not to be made larger; if the I_{SC} exceeds the upper bound of $I(^*)$, the cover shall be kept the same.
6. The final width of the shadowed area, paired with the position of that area that shade the cells which show the lowest current, results in the worst case shadowing condition. This shadowed area will be used for hotspot testing.
7. Withdraw the cover and inspect the module visually.
8. Measure the module I-V characteristic again and determine the maximum power P_{max2}.
9. Place and put the cover on the module at the position determined in steps 5) and 6).
10. Put the module in short-circuit conditions and also include a means to monitor the module current.
11. As described in Step 1, expose the module to the steady-state radiant source providing a total irradiance of (1000 $\pm$ 100)W/m^2 at the module surface, using either source (b) or (c).

12. For this test, the temperature of the module shall be in the range (55 $\pm$ 15) °C. Note the value of I_{SC} and make sure that the module current stays above the lower limit of $I(^*)$. If it falls below the lower limit, decrease the width of the shadowed area in increments of one cell width until I_{SC} once again exceeds the lower limit for $I(^*)$. If the current falls below the desired range but the minimum area is already reached, no adjustment shall be made.
13. These conditions have to be maintained for an exposure time of 1h.
14. Finally, determine with the help of an IR camera the hottest area on the shadowed cells.

And as last, the requirements to pass this test are as follows:

- No evidence of major visual defects (as defined in Clause 7).
- The degradation of the P_{MP} shall not exceed 5% of the value measured before the test.
- Insulation resistance shall meet the same requirements as for the initial measurements.

2.2.3. Literature

To the best of my knowledge, no detailed literature was available on hotspot formation and associated failures in thin-film a-Si modules. Hence, the background literature review that was available on c-Si technologies was utilized in the experiments. But first, the differences between the two have to be understood.

Single c-Si is made out of a perfect crystalline lattice, in which every silicon atom is tetrahedrally bonded to four other silicon atoms [10]. On the contrary, a-Si has a so-called continuous random network. In the short-range order on atomic length scales, the atom of a-Si still has a tetrahedral coordination structure, just like its silicon counterpart, but in long-range order, the lattice does not look crystalline anymore. That is because the silicon-silicon bond lengths and the bond angles are slightly distorted when compared to a c-Si network. As a result, not all silicon atoms in a-Si have four silicon neighbors. A schematic drawing of both structures can be seen in Figure 2.3.

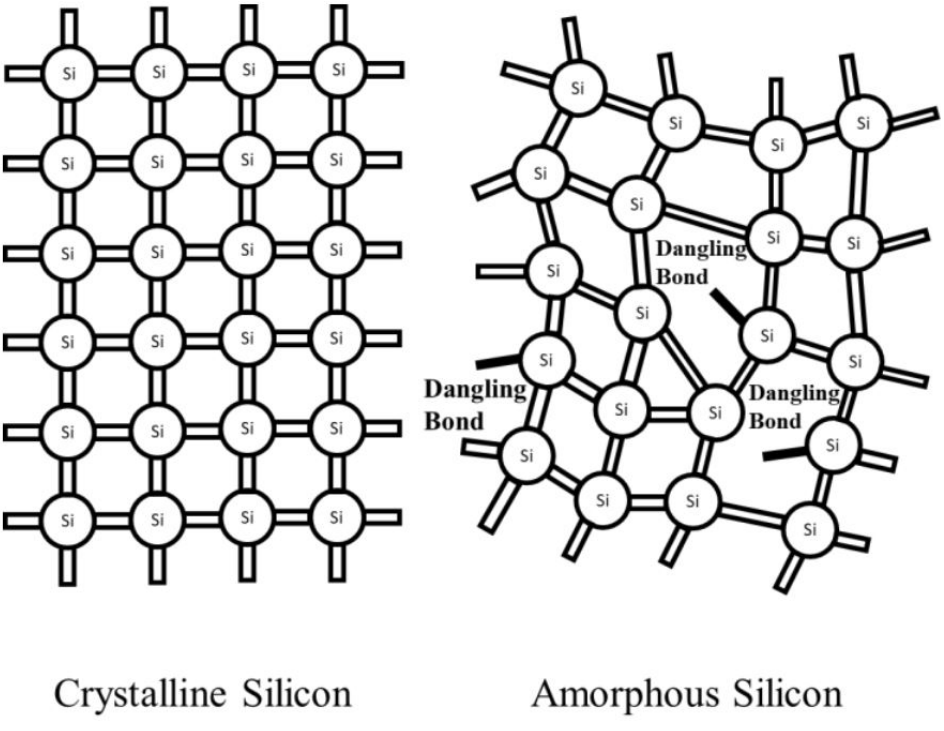

Figure 2.3: Schematic structure diagram of c-Si and a-Si network [11]

Because the lattice for a-Si is random and silicon has four valence electrons, not all valance bonds are connected to other silicon atoms, which results in dangling bonds. These bonds are also defects and because of that, a-Si has a much higher defect density than c-Si, being $10^{19}/cm^3$ and $10^{14}/cm^3$ respectively. This causes a-Si to have poor conductivity when compared to c-Si because the defects

lead to fast recombination of photoexcited charge carriers. c-Si has a bandgap energy of 1.1 eV and is indirect, whereas a-Si has a direct bandgap material. The bandgap of a-Si ranges from 1.6-1.8 eV depending on the dangling bonds density. From Figure 2.4, it can be seen that c-Si and a-Si both start absorbing photons at the bandgap energy of 1.1 eV. Although bandgap energy of a-Si is higher than that of c-Si, the defect states and band tails of a-Si allow electrons to excite at low photon energies. It also can be seen that starting from 1.8 eV, the absorption coefficient of a-Si becomes at least an order of magnitude higher as compared to c-Si. This is due to the direct bandgap nature of a-Si. This results in a-Si absorbing much more than c-Si in the visible and UV part of the spectrum, which makes a-Si suitable for thin film solar cells.

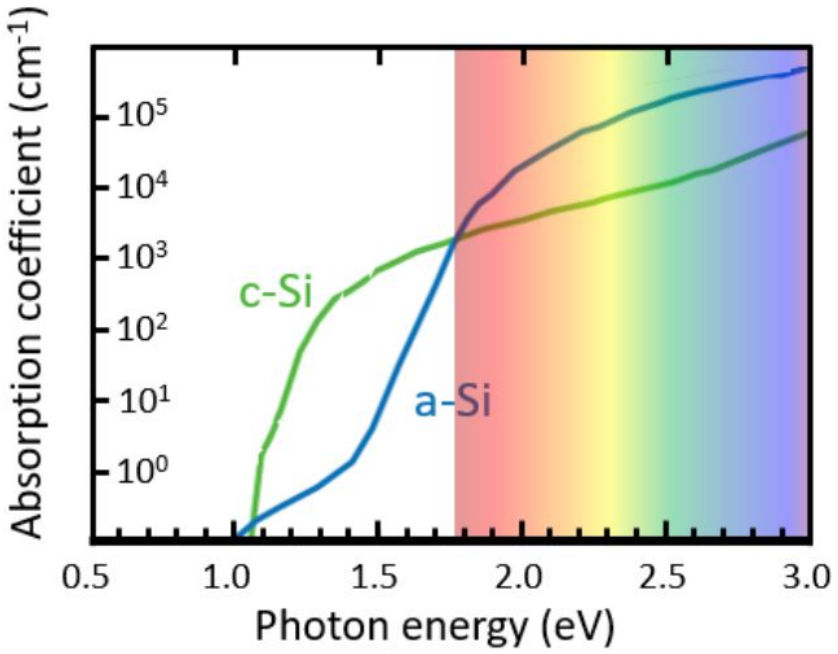

Figure 2.4: The absorption coefficient of both c-Si and a-Si as a function of photon energy [10]

Both c-Si and a-Si have different potential applications [11]. When space is limited and the price is a concern, c-Si solar modules would be the more appropriate choice. They have higher conversion energy, meaning the area required to produce a certain output is lower than a-Si solar modules. Also, the cost per watt of c-Si solar cells is half or less when compared to a-Si solar cells [11]. One of the conditions in which a-Si is more favorable is for artificial (indoor) light conditions. Because of its higher absorption coefficient of artificial light sources than c-Si, it is the better choice. Also when looking at weight-related factors and design aesthetics, a-Si is the better choice. The cells are thinner and the weight density is lower than c-Si, so a-Si cells do not put excessive weight on buildings. Furthermore, a-Si cells are flexible, which allows seamless integration on different types of rooftops and into devices.

The interconnection between cells in a module is also of importance, as that can be a potential candidate region for defect formation. The interconnection of the batch of modules from HyET can be seen in Figure 2.5. At first, the aluminum foil, TCO and a-Si are deposited on top of each other. Secondly, scribes are made that go through the TCO and silicon layer, called the P1 scribe (P1s). Afterward, these scribes are filled with an insulating ink, called P1f. This filling ensures that the solar cells are isolated from each other. Subsequently, another scribe is made that only goes through the silicon, called the P2s, and another ink (P3f) is applied on top of the silicon. The purpose of the P2s is to connect the cells with each other and should have low resistance. Then, the back contact is made on top of the silicon and P3f, filling up the P2s in the process. Subsequently, the P3f is lifted off along with the back contact, leaving scribes in the back contact called P3, which separates the back contact of the cells. Finally, a lamination is made using the PEN and deposited on the back contact, filling up the P3 scribes, and the aluminum foil is etched away except from the busbar area. The black arrows indicate the current flow, so from the P3 side to the P1s side. Keep in mind that the size of the active

region and the interconnection are not representative.

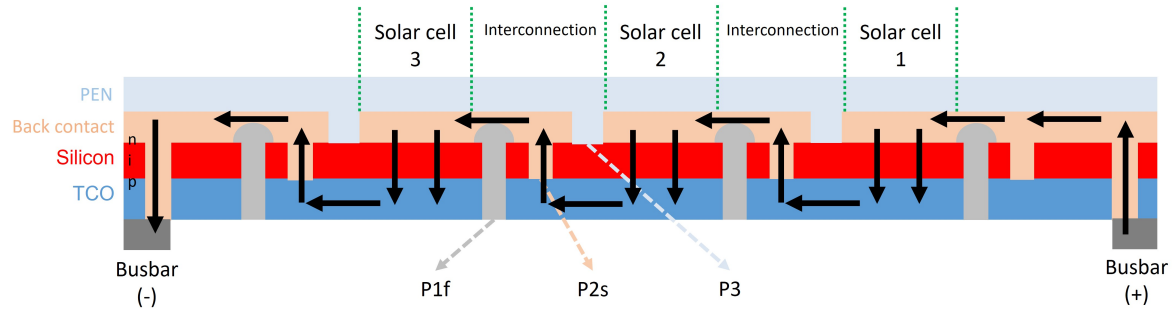

Figure 2.5: Schematic representation of the cross-section view of HyET device architecture. The black arrows indicate the current flow, flowing from the P3 side to the P1s side. The P1f scribe divides the cells, the P2s scribe connects the individual cells with each other and the P3 scribe separates the back contacts of the cells

As mentioned before, little to no research has been reported about hotspots for a-Si in recent years. Consequently, some literature study about hotpot formation in c-Si modules has to be done in order to get an understanding of what can be expected for a-Si modules.

According to Simon and Meyer [12], their results revealed a direct correlation between areas of high impurity contaminants and hotspot heating that can be noticed in different multicrystalline solar modules. They attributed the presence of oxygen, carbon, iron and platinum to the hotspot formation for these cells. It is recommended to minimize oxygen and transition elements in order to increase life expectancy and overall improve system reliability. Another study suggested that hotspot formation can be prevented by introducing a new bypass circuit [13]. This circuit has an 'analogical' behavior, meaning it self-activates when mismatch conditions occur and it does not require other complex logic circuits or microprocessors. Furthermore, according to the report, the worst case operating conditions as defined in EN 61215, a difference has been found of 50°C between a shaded cell protected by a standard bypass diode and a shaded cell protected by the new bypass circuit under the same operating conditions. A bunch of studies [14]–[18] also go into depth about defect analysis for various solar modules (c-Si, thin-film, etc.) by using electroluminescence and infrared (IR) thermography. They all conclude that these are good methods to view different kinds of failures and defects. Furthermore, these reports also give a deeper insight into the role of EL in diagonalizing the modules. There is also a report that concludes that the performance of thin-film solar modules is better under partial shading conditions than c-Si modules [19]. Lower hotspot damages are observed in thin-film modules, which is because of the inherent orientation (monolithically integrated cells) and super junction properties [19].

3

Methodology

In this chapter, the identification of the WCSS will be explained. After that, different light soaking methods which were used during the thesis are discussed. Finally, different characterization methods are mentioned.

3.1. Identifying the worst case conditions

Following steps 1-7 as explained in Chapter 2.2.2, the WCSS was determined for two solar modules with the use of the LASS (more about the LASS in Chapter 3.3.1). Two highly degraded modules were chosen from a batch of numerous modules from HyET based on their performance and I-V characteristics. The IEC 61215 norms suggest that the WCSS is selected by measuring the worst I_{SC} value using a multimeter. However, in this case, a complete I-V measurement was conducted and the WCSS was identified based on the lowest I_{SC} value extracted from the I-V curves. During this step, the modules were illuminated for around 30 seconds to 1 minute per I-V measurement. During these measurements, the temperature was around 30-33°C. Shading of the cells was done by using a black piece of paper and during the process of identifying the WCSS, it became apparent that for all two of the modules, the mask width was two cells. With that, the two worst cells in each of the two modules were determined and steps eight through fourteen were carried out at a later date at HyET in their light soaking machine.

3.2. Light soaking

Once the WCSS is identified, the next step is to light soak the modules at SC conditions to check for the possibility of hotspot formation. This step is done in two places: at HyET and at the TU Delft. Each of the light soaking procedures is explained as follows.

3.2.1. Light soaking at HyET

In order to execute steps 8-14 for the hotspot endurance test, the light soaking machines at HyET were used, which can be seen in Figure 3.1. These machines have a set irradiance of 1000 W/m^2. However, during the 1 hour of light soaking, the intensity was varying over the range of 950-1050 W/m^2. They also have a cooling unit that keeps the module at 50°C. Here, the two worst cells of each module were shaded and put inside the machines. The light soaking experiment was done at both OC conditions and at SC conditions. Although the IEC Certification states that it only should be done at SC conditions, a test at OC conditions was also carried out to see if only temperature would have had an effect in creating hotspots.

Figure 3.1: Light soaking machines at HyET which were used for light soaking the modules at OC and SC conditions

3.2.2. Light soaking at TU Delft

Besides using the light soaking machines at HyET, there is also a light soaking machine available in the ESP Lab of TU Delft. This machine has a cooling unit that keeps the temperature of the module around 50°C, but it has a maximum set irradiance of 720 W/m^2, varying from 700-720 W/m^2 across a 30cm x 30cm surface area. This is not as per the IEC 61215 norm, however, it has a different light spectrum and provides similar I_{SC} values as that at HyET. Furthermore, this system is routinely used for light soaking studies at the TU Delft. These were used to see if different defects in cells in EL images would result in hotspots when shaded; numerous areas of two cell width would be shaded one by one for one hour in SC conditions. Results from this machine can be found in Chapters 5 and 6 The light soaking machine and the experiment's setup can be seen in Figure 3.2.

(a) Outside of the machine

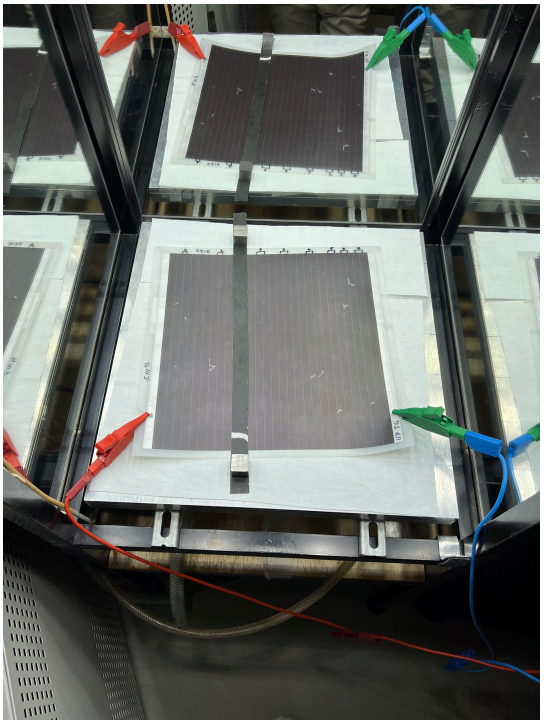

(b) Inside of the machine

Figure 3.2: Light soaking machine at TU Delft and the experiment's setup. It was used to light soak modules with shadowed cells that have defects in them to see if they turn into hotspots.

3.3. Characterization methods

3.3.1. LASS I-V Tracer

The LASS is a large-area solar simulator that is used to measure the I-V curves of solar modules. The setup is shown in Figure 3.3. This solar simulator was used to determine the WCSS, trace the I-V curve and extract all important parameters, like I_{SC}, V_{OC}, FF and the efficiency. The software used to get all the values is called *ReRa Tracer 3*. The LASS has an irradiance between 950-1050 W/m^2 and comes with a temperature probe to measure the temperature of the modules. Because the LASS does not have a cooling system. Hence, it is not suitable for light soaking at a fixed temperature (as mentioned in the IEC norms) for thin-film a-Si modules. The modules heat up really quickly to temperatures above 50°C within 5 minutes, it is not suited for light soaking. As the LASS is a custom-built machine for the TU Delft, it does not have a datasheet, but it does have the following important specifications [20]:

- **Spectral Match**: Class C. Spectral mismatch is a measurement of the distribution of white light across six different wavelength ranges as a percentage of the total irradiance; in this case, the ideal acceptable range ratio is 0.4-2.0%.
- **Spatial Non-Uniformity**: Class A. Spatial uniformity shows how the irradiance varies over a certain area. For Class A, the non-uniformity of irradiance is 2%.
- **Temporal Instability**: Class A. To not distort the measurements, the output of the solar simulator must be stable over time. For Class A, the temporal instability is 0.5%

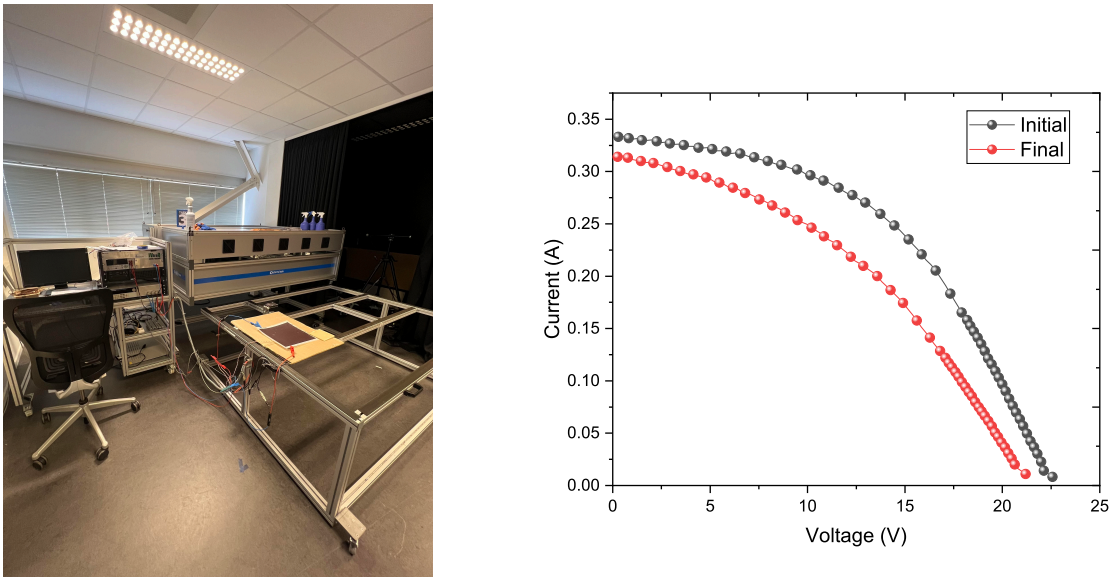

(a) (b)

Figure 3.3: On the left is the LASS setup used to do the WCSS, as well as get the I-V curves and important parameters. On the right, I-V curves are given of the initial and final values after hotspot light soaking obtained by the LASS

3.3.2. Phone images

Images are taken with an iPhone 13 Pro camera. After each procedure, a couple of images of the frontside and backside of the modules are taken. This was done in order to keep track of when each hotspot was created and as a representation for visual inspection. An example is shown in Figure 3.4.

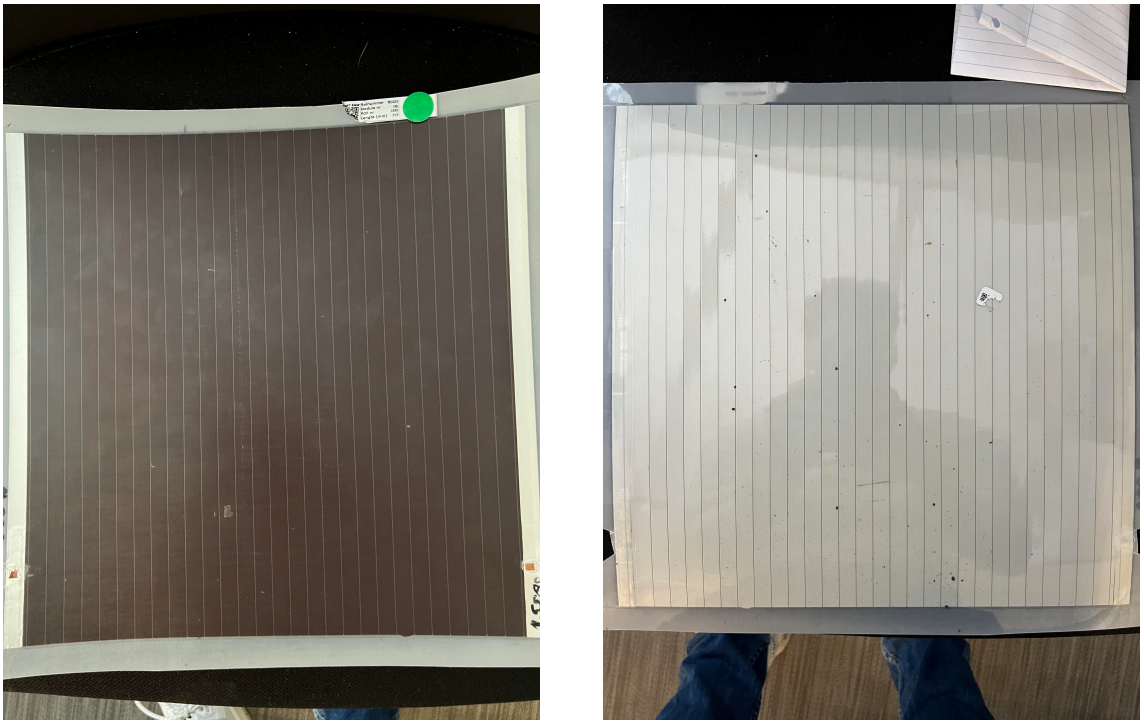

(a) (b)

Figure 3.4: Front and backside of module R20026-4096 taken by the iPhone 13 Pro camera.

3.3.3. EL imaging

Electroluminescence is an electrical and optical phenomenon in which an electric current or strong electric field passes through a material, which results in the material emitting light. In this case, a current is fed into the module which causes light emission because of radiative recombination of carriers. EL is a non-destructive and relatively fast way to get a wealth of data about the cells in the module. The image produced is gray-scale and the intensity of the light is exponentially proportional to the local voltage, meaning that the brighter the cells are in the image, the better and the darker the cells, the worse, as can be seen in Figure 3.5. Dark cells in the image imply they still produce power, but far less than the cells that are white in the images. Shunts and recombination centers can also be seen in these images. EL imaging is used for the progress of the cells after each procedure to see if they have gotten worse (darker) over time and to predict which cells are likely to produce hotspots when shaded.

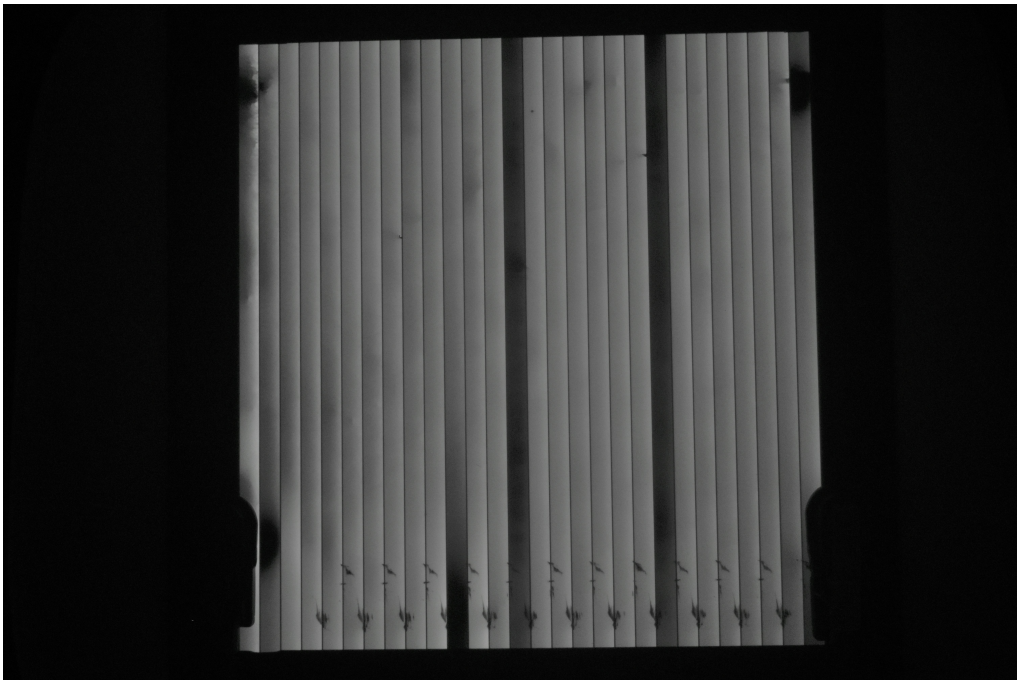

Figure 3.5: EL image of one of the HyET modules taken at its I_{SC} value. The brighter the cells, the more voltage goes through them and thus the better the cells are.

EL images were taken at 100%, 80%, 60%, 40%, 20% and 10% of the modules' I_{SC}, as to see if there were any shunt defects visible. The camera used is a *Nikon D7200* and is equipped with an *AF-S NIKKOR 28mm f/1.8G* lens and an IR filter in front of the lens. Furthermore, the software *Camera Control Pro 2* was used to control the camera and its setting, which were as follows:

- **Exposure Mode**: Manual
- **Shutter Speed**: 2 min
- **Aperature f/1.8**
- **ISO**: 1000
- **White balance**: preset manual d-1

In order for EL imaging to work, the camera and module have to be placed in a dark small room. The setup is shown in Figure 3.6.

(a) (b)

Figure 3.6: Camera setup in the PV Lab at TU Delft used for EL imaging

3.3.4. IR imaging

IR imaging is used during the light soaking to capture the temperature variation across the modules. The infrared camera used is the *Fluke Ti32 Infrared Camera* (Figure 3.7a). This camera produces images that give a clear overview of the temperature differences within the images, also providing a temperature scale that is fitted for the image, as shown in Figure 3.7b. This Figure shows a module being shadowed by a strip of paper, indicated by the long vertical rectangle. It also contains two hotspots as indicated by the two yellowish/white circles. Furthermore, the *Fluke 568 Infrared Thermometer* (Figure 3.8) was also used to validate the temperature maps obtained by the IR images.

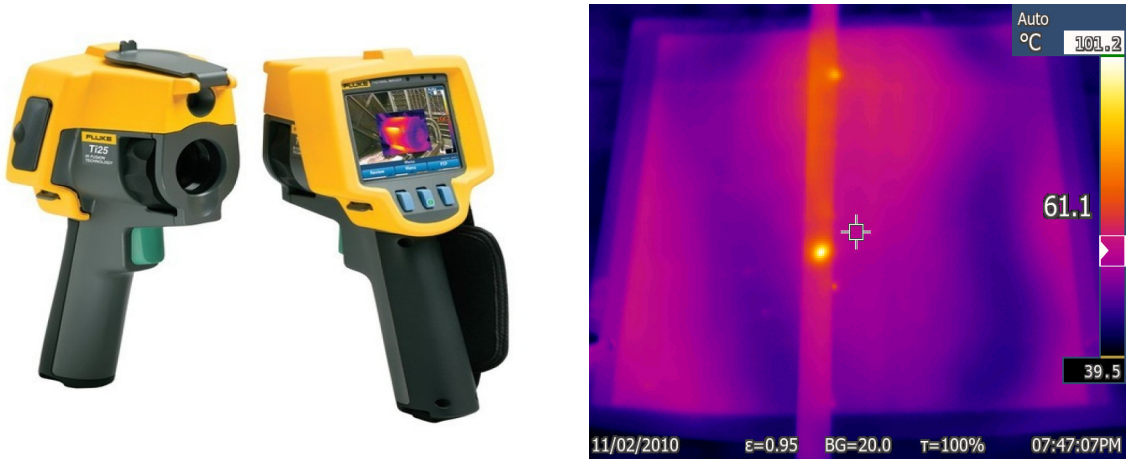

(a) (b)

Figure 3.7: The Fluke Ti32 IR Camera [21] is seen on the left image and an image produced by the camera can be seen on the right. This camera was used to see the temperatures of the hotspots, as well as to see when they were created. The strip of paper used to shadow the cells can also be seen as a long, stretched-out rectangle

Figure 3.8: Fluke 568 IR Thermometer [22]. This thermometer was used to measure the temperature, but also to validate the temperature map produced in the images from the Fluke Ti32 Camera.

4

Hotspot endurance testing of thin-film a-Si modules

This chapter will show the first part of three of the results. This section will present the results of hotspot formed in thin-film a-Si modules after the IEC 61215 certification norms. Two highly degraded modules are used for this procedure. Hotspots are both inspected visually and by EL imaging. A comprehensive analysis based on these inspections is presented.

4.1. Solar module selection

From the available batch of thin-film a-Si modules, two highly degraded samples were selected for testing their endurance to hotspots asper the IEC 61215 norms. The most degraded solar foils were selected assuming that these modules have a higher probability of producing hotspots than in less aged or degraded modules. The two modules that were chosen are: *R20026-4096 & R20026-3932*. The extent of degradation was decided based on the I-V external parameter extracted from the I-V measurements of the LASS. In the process of determining these, it was noticed that the modules became hot, even after a couple of seconds under the light. The temperature probe indicated that the temperature of the modules would reach between 40-50°C. Because the modules had to undergo multiple measurements to better determine the parameters, there were intervals of 5 minutes between measurements in order to cool down the modules to around 30°C. It was observed that apparently to reach 25°C, it took nearly 20 minutes to reach this temperature. Hence, all the I-V measurements were done at 30-33°C to make sure the variation in the external parameters was minimal. The initial EL and normal images of the two modules can be seen in Figures 4.1 & 4.2 below. In the EL images, irregularities in the solar module can be seen. From Figures 4.1b and 4.2b, the regions marked inside the green circle show defects that are turned into hotspots later after the light soaking. However, these defects were not visible by visual inspection as seen in Figures 4.1a and 4.2a.

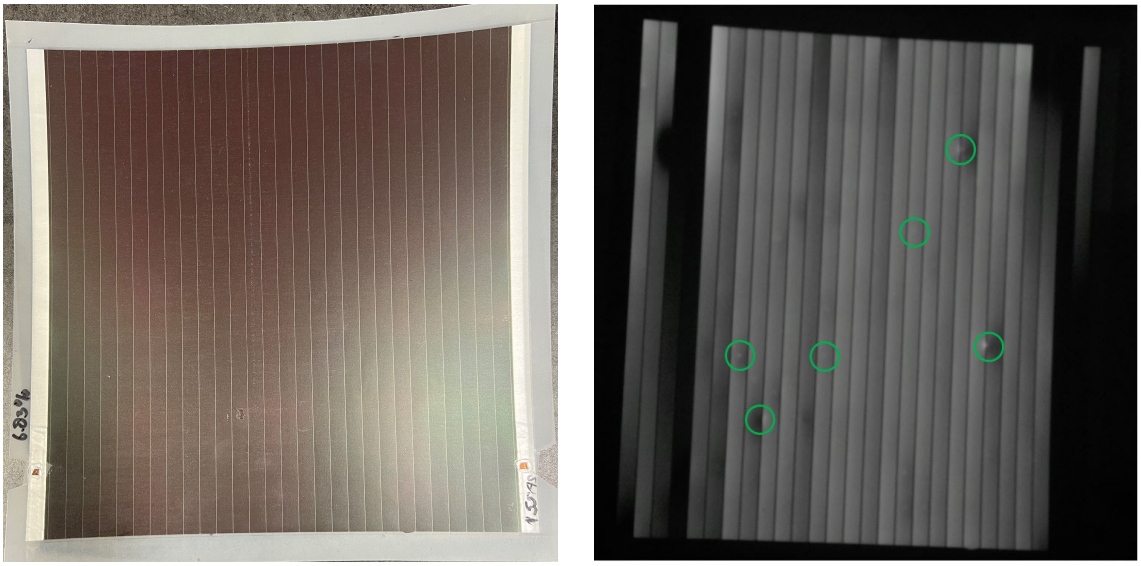

(a) Phone Image **(b)** EL Image

Figure 4.1: Represents the initial photograph and EL images of R20026-4096 thin-film a-Si module used for hotspot testing.

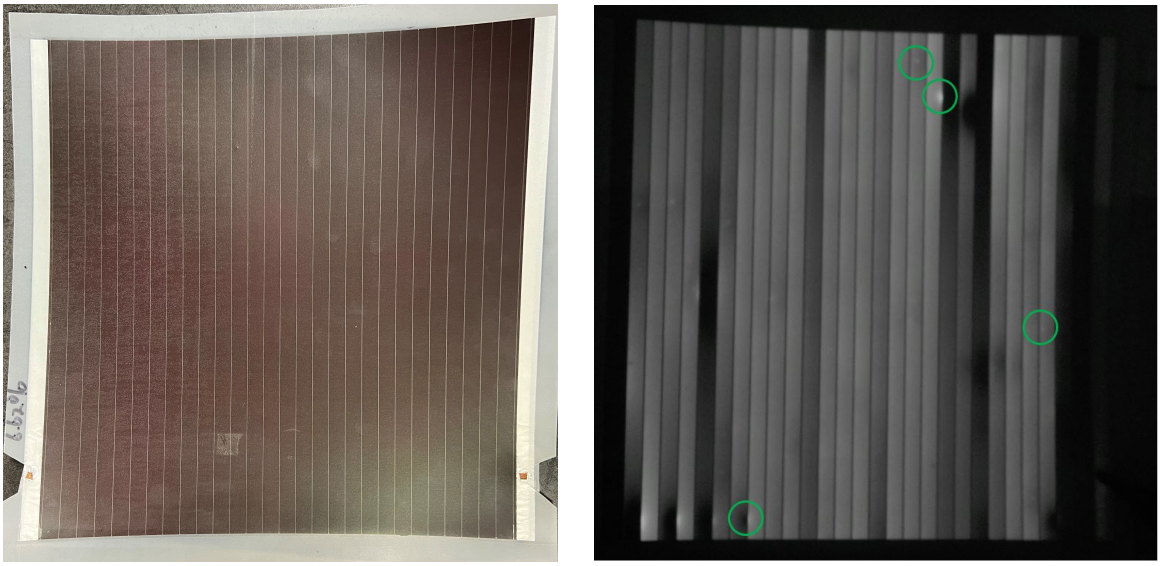

(a) Phone Image **(b)** EL Image

Figure 4.2: Represents the initial photograph after visual inspection and EL images of R20026-3932 thin-film a-Si module used for hotspot testing.

4.2. Worst case shadowing scenario

To determine the WCSS for the two modules, the procedure explained in Chapter 2 was followed. At first, the unshadowed I-V curve and parameters of the modules were determined again with the LASS. Then, the modules get shaded by black pieces of paper with different cell widths. Initially, black paper with a width of four cells was used. As per the IEC Procedure, if the I_{SC} gets below the range of $I(^*)$, the width has to be reduced until it is back in the range. If the width used is two cells wide and still below the range, continue doing the shadowing measurements with a width cover of two cells. For both modules, it became apparent that the width had to be two cells. Also, as explained before, the modules get heated up pretty quickly when exposed to the LASS, which influences the temperature and thus the parameters. To make sure that the temperature fluctuations have minimal effect on the measurements, there were gaps of 5 minutes between measurements for the modules to cool down to

around 30-33°C, and two to three measurements were done per position of the cover. After finishing shadowing the modules, the WCSS were determined by looking at which combination of two shadowed cells gave the lowest I_{SC} values. For *R20026-4096*, these are cells 10 & 11 and for *R20026-3932* cells 13 & 14. The EL images after this procedure can be seen in Figure 4.3.

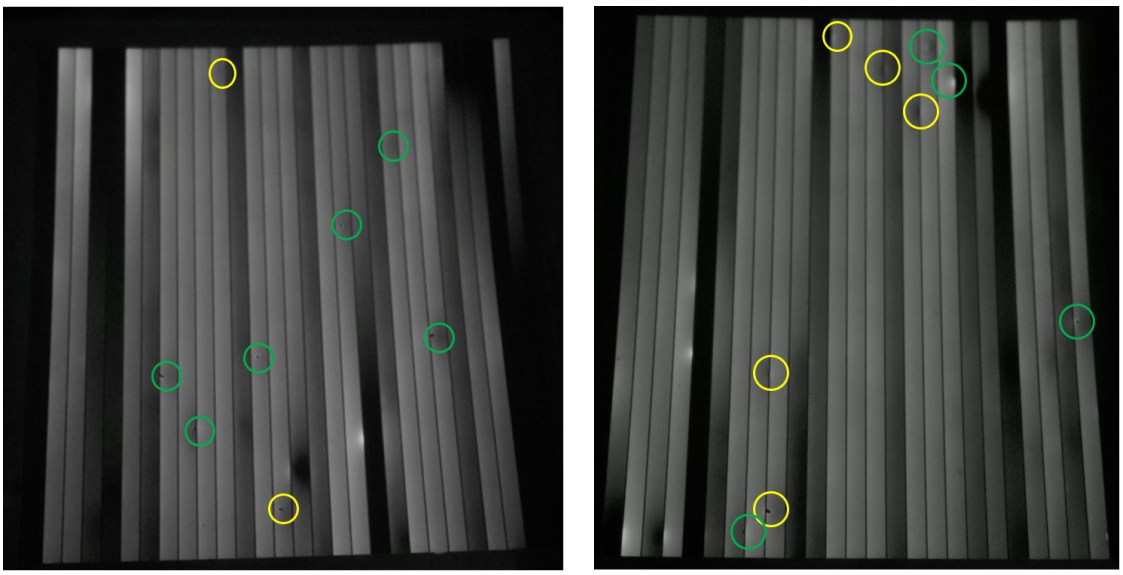

(a) R20026-4096 **(b)** R20026-3932

Figure 4.3: Represents the EL images of both R20026-4096 and R20026-3932 taken after the WCSS

When comparing the EL images with the as-received samples, some differences can be noticed. Both modules have cells or part of the cells turned dark and some cells have an additional bright spot. Furthermore, the yellow circles indicate irregularities that will turn into hotspots later on. These were formed during the WCSS procedure. Some of them already seem like hotspots if the circle indicates a black spot, which means no silicon is present there. Also, it is observed that other circles have white dots or areas with high or very low light intensity.

4.3. Light soaking at open-circuit conditions

Light soaking was done at HyET Solar with their light soaking machines (Figure 3.1), as these are up to standard according to the IEC procedure. Both solar modules were put in these machines for one hour each, at set conditions of 1000 W/m^2 illumination and 50°C with the two worst cells being shadowed by the piece of black paper used for the determination of the WCSS. At this time, the modules were not connected to a multimeter, so both modules were in OC conditions. The images below (Figures 4.4 & 4.5) show EL and photograph after visual inspection of both modules after the light soaking at OC conditions for 1 hour. The arrow in the images indicates which two cells have been shaded during the light soaking procedures.

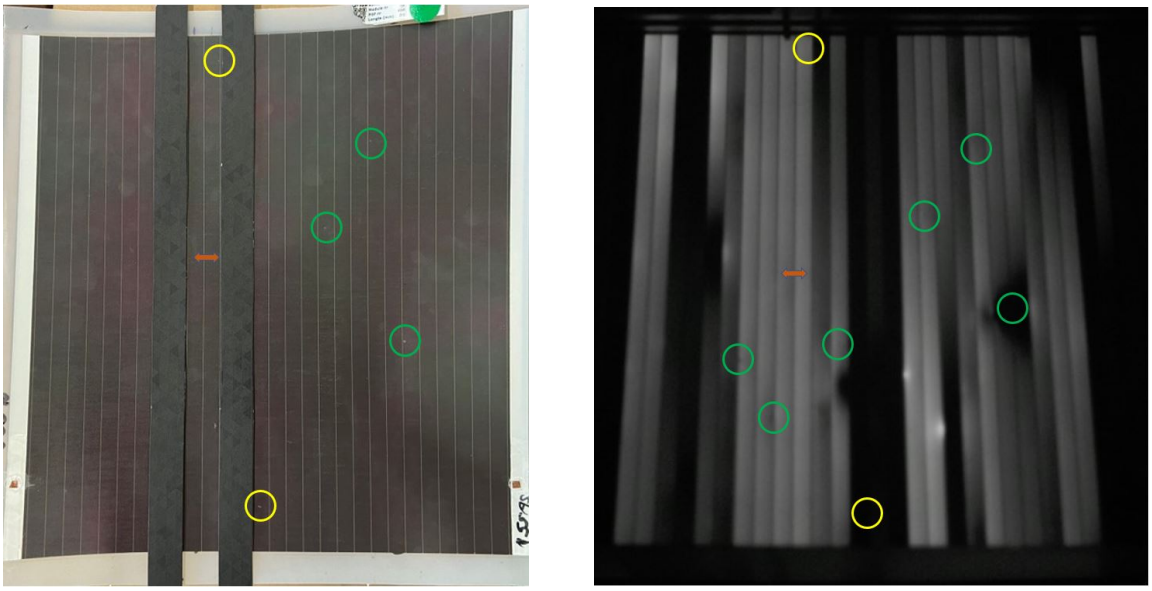

(a) Phone Image **(b)** EL Image

Figure 4.4: Represents the photograph after visual inspection and EL images of R20026-4096 after light soaking at OC conditions.

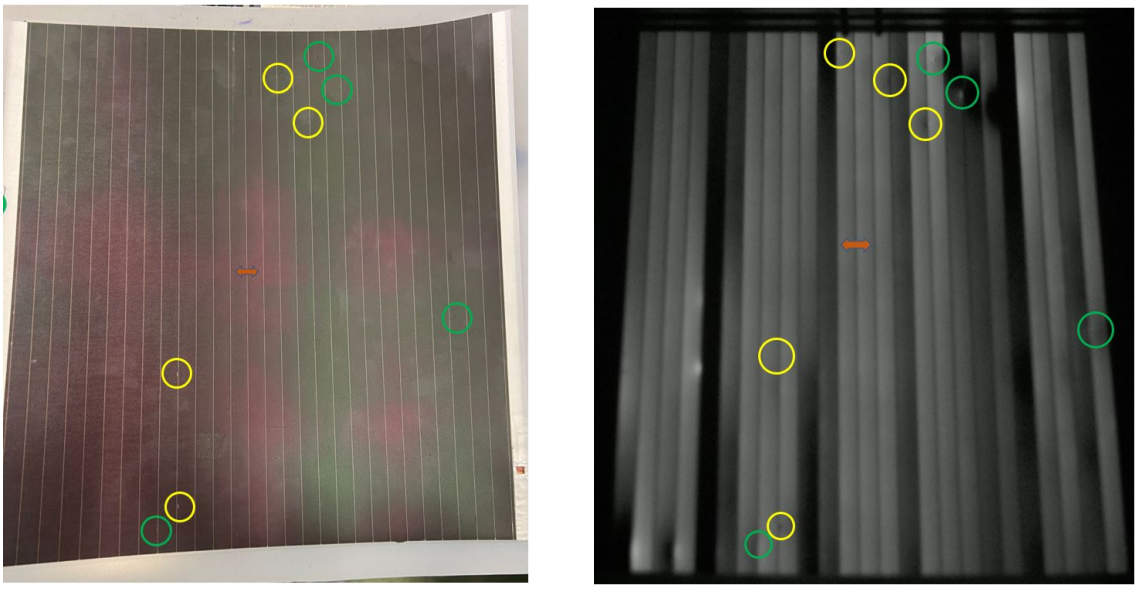

(a) Phone Image **(b)** EL Image

Figure 4.5: Represents the photograph after visual inspection and EL images of R20026-3932 after light soaking at OC conditions.

From Figures 4.4a and 4.5a, hotspots can now be seen visually. The hotspots were formed by the defects/irregularities that are indicated by the green and yellow circles visible in the EL images. It is believed that these hotspots were the result of the WCSS procedure and not during the light soaking at OC. That is because, during OC light soaking, only two cells are shadowed with no current flowing through the module, and during the WCSS procedure, every cell gets shadowed and illuminated at SC conditions for half a minute, which may be long enough to create hotspots.

4.4. Light soaking at short-circuit conditions

Here, the same process is carried out as light soaking at OC, but this time, it will be executed at SC by connecting a multimeter across the solar modules. The photograph after visual inspection and EL images of R20026-4096 and R20026-3932 are shown below in Figures 4.6 & 4.7 respectively.

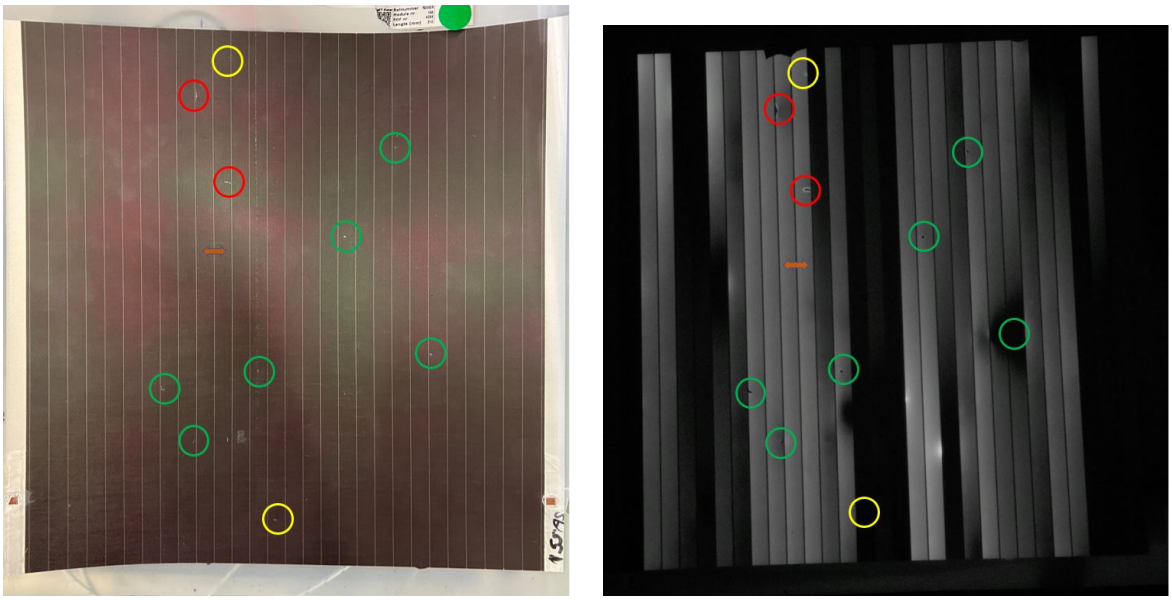

(a) Phone Image **(b)** EL Image

Figure 4.6: Represents the photograph after visual inspection and EL images of R20026-4096 after light soaking at SC conditions.

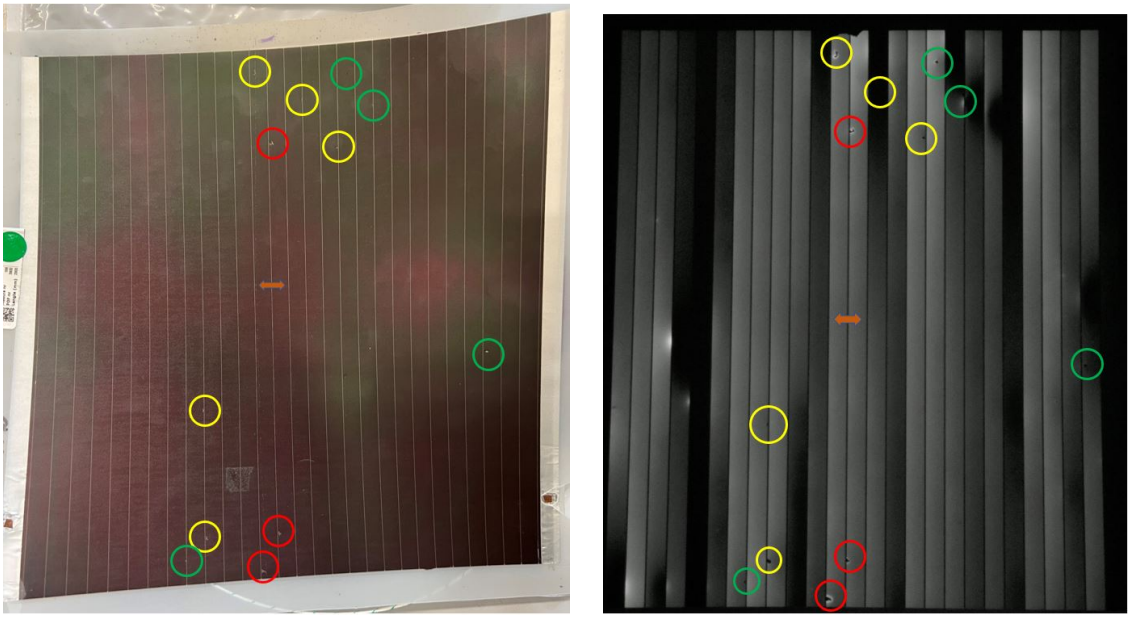

(a) Phone Image **(b)** EL Image

Figure 4.7: Represents the photograph after visual inspection and EL images of R20026-3932 after light soaking at SC conditions.

Now, as opposed to the previous procedure, hotspots did form in the shadowed area. All of these hotspots, apart from one, did not have any prior defect from the EL images that could indicate that a hotspot would form there. Figure 4.8 gives an overview of the I-V curves of both modules after each

procedure. It can be seen that both modules have degraded further, with R20026-4096 degrading more than R20026-3932. Figure 4.9 shows several zoomed-in images of hotspots created during the WCSS and during light soaking at SC conditions. As seen in the images, the hotspots created during WCSS are more of the circular type, while those created during the light soaking are bigger and linear.

Figure 4.8a and 4.8b visualize during which procedure the defects/hotspot became apparent in EL images and photographs, respectively.

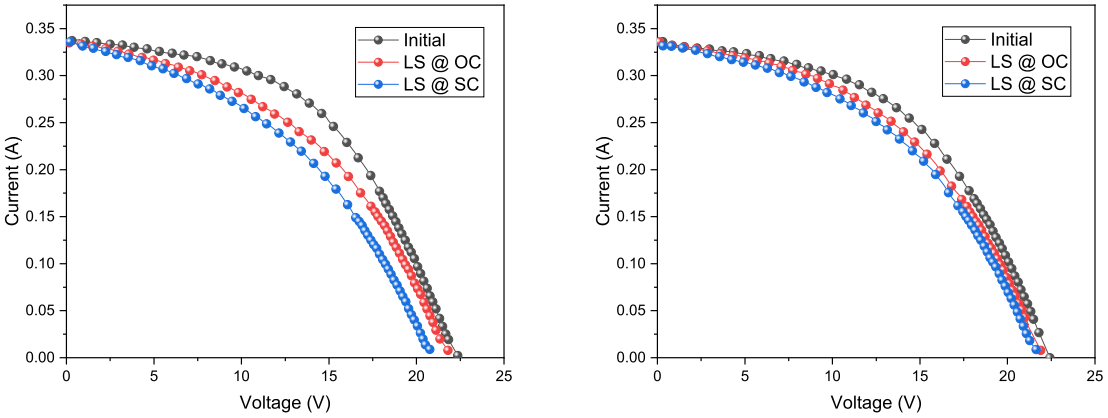

(a) I-V curves of R20026-4096

(b) I-V curves of R20026-3932

Figure 4.8: Represents the I-V curves of R20026-4096 and R20026-3932 after the procedures.

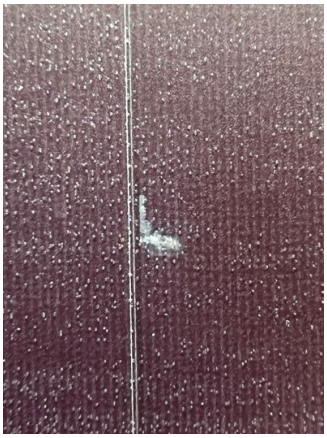

(a) Frontside image of a hotspot created during WCSS on R20026-4096

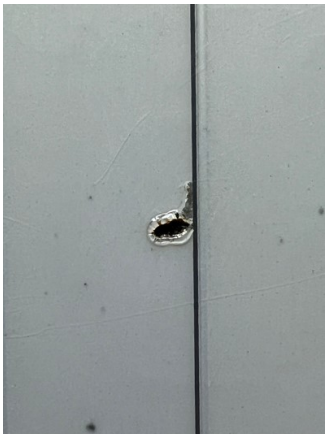

(b) Backside image of a hotspot created during WCSS on R20026-4096

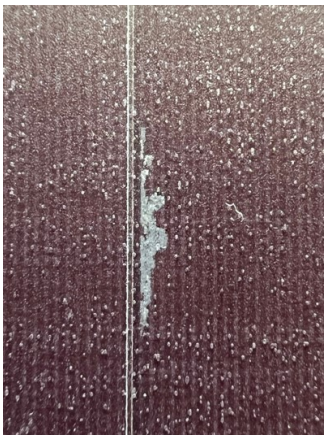

(c) Frontside image of a hotspot created during LS at SC on R20026-4096

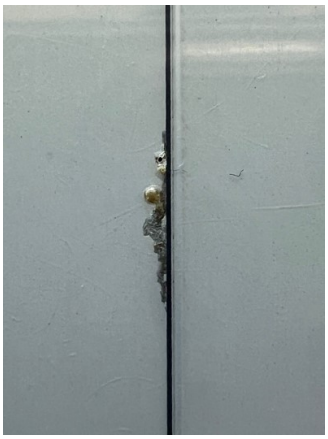

(d) Backside image of a hotspot created during LS at SC on R20026-4096

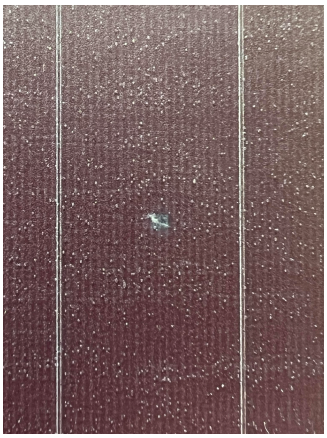

(e) Frontside image of a hotspot created during WCSS on R20026-3932

(f) Backside image of a hotspot created during WCSS on R20026-3932

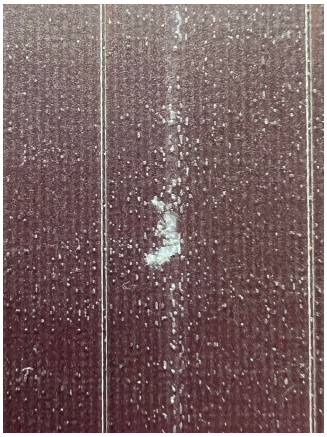

(g) Frontside image of a hotspot created during LS at SC on R20026-3932

(h) Backside image of a hotspot created during LS at SC on R20026-3932

Figure 4.9: Zoomed-in images of the frontside and backside of hotspots present on R20026-4096 and R20026-3932

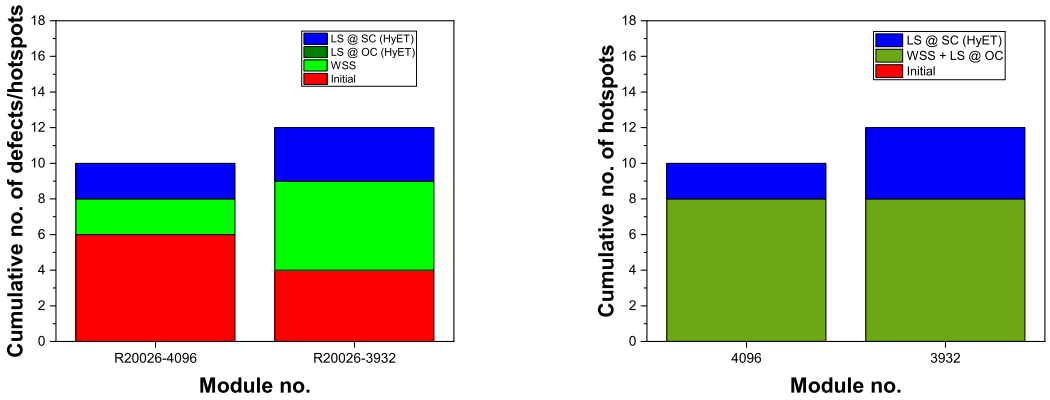

(a) Defects/hotspots visible in EL images

(b) Hotspots visible in phone images

Figure 4.10: Visualization when defects and hotspots became visible in phone and EL images after which procedure.

Looking at Figure 4.10a, out of the 10 hotspots formed in R20026-4096, six of them had the presence of predictor defects in the initial EL image. Then two hotspots each were formed during the WCSS procedure and light soaking at SC without any predictor defects. In contrast, R20026-3932 had only shown four predictor defects that were visible initially on the EL image that turned into hotspots later on during the WCSS and light soaking procedure. Out of the four hotspots that were formed after SC light soaking, only one of them had a defect predictor prior to that procedure that was formed during WCSS. From Figure 4.10b, zero hotspots were seen during initial visual inspection and eight hotspots became visible after the WCSS and light soaking at OC conditions. Because there are no images captured after visual inspection after the WCSS, it has been categorized together with light soaking at OC. However, as explained before, it is highly likely that the hotspots that occurred have been caused during the WCSS procedure. Finally, two hotspots formed during the light soaking at SC conditions. So, of the ten hotspots that are present on R20026-4096, eight of them were already noticeable by defects before being created. For R20026-3932, eight of the twelve hotspots formed originated from the predictor defects.

5

Defects and their susceptibility to hotspot formation

This chapter focuses on the classification of the different kinds of defects that lead to the formation of hotspots during light soaking at SC conditions. A probability map is also generated to see how often these predictor defects turn into hotspots based on limited experiments.

5.1. Classification of defects

As seen in the previous chapter, hotspots have formed in many cases from predictor defects that can be seen by EL images. In order to get a better understanding, these defects have been classified into three groups, which are: *Current crowding*, *White dots* and *Dark region*. An example of these defects can be seen in Figure 5.1 below.

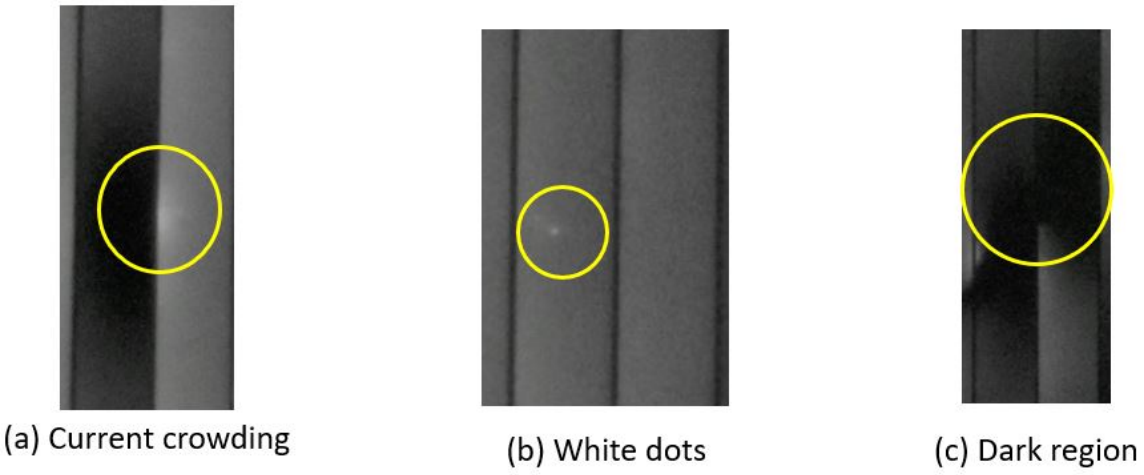

Figure 5.1: Represents the three different kinds of defects that are present in EL images

Current crowding is a defect that is indicated by a brighter contrast region. This was always present at either side of the scribes. A white dot is self-explanatory; it is a small dot that is slightly lighter than the cells on the EL images and can be found anywhere in the cell. A dark region in a cell gives off a lower contrast in EL images. These dark regions can be a specific region in the cell, a significant portion of the cell, or the full cell itself. It can either be a recombination region or a shunt path. Current crowding and dark regions were always present in combination. If current crowding is visible on the right scribe of a cell, then a dark region is present on the next cell adjacent to the current crowding. The same also occurs when the current crowding is on the cell's left scribe, then the dark region is adjacent to the current crowding on the previous cell.

5.2. Procedure

Now that it is known that hotspots can be formed from these kinds of defects, it is also essential to understand how often these defects will turn into hotspots. In order to do that, two other modules from the same batch (which underwent light soaking and annealing at OC conditions prior to hotspot endurance testing) were used to determine this probability. With EL imaging, eight to nine pairs of cells per module were chosen that contained a combination of these defects and were each individually shaded for an hour during light soaking at SC conditions using the light soaking machine at the TU Delft. Two additional degraded modules from the same batch have been used during this experiment: *R21020-3137* and *R20026-4552*. This experiment is carried out in two steps. In the first step, six areas per module (a combination of two cells) were shadowed and light soaked at SC conditions. In the second step, additional areas for shadowing were selected based on the defects to generate more data and underwent light soaking under the silimar conditions.

5.2.1. First round

Prior to this experiment, these modules underwent an annealing and light soaking process at OC conditions for a couple of hours in order to investigate the Staebler–Wronski Effect. This, however, did not impose any problems for the experiment. As mentioned previously, the pairs of cells to be shaded were chosen based on the EL images, which can be seen in Figure 5.3. Photograph after visual inspection of the modules before the experiment can be seen in Figure 5.2. The two yellow circles that can be seen in Figure 5.2b indicate two hotspots that were caused during EL imaging; the module was in reverse bias at high voltage for a period of time, causing the defects (white dots) to form into hotspots.

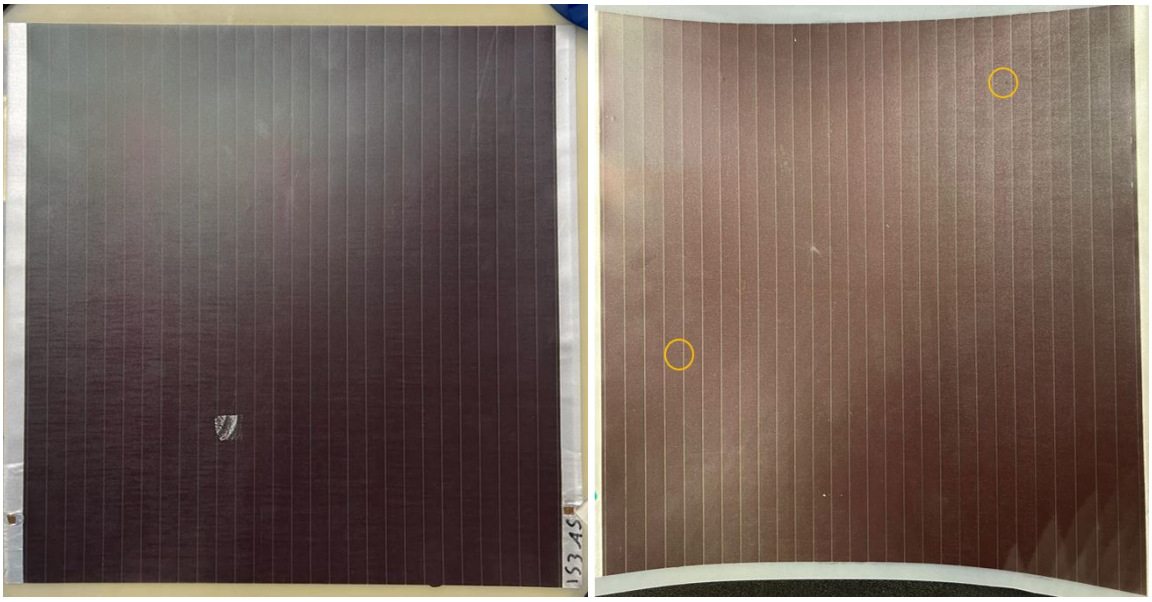

(a) R20026-4552 **(b)** R21020-3137

Figure 5.2: Represents the photograph after visual inspection of R20026-4552 and R21020-3137 right before starting the light soaking experiment

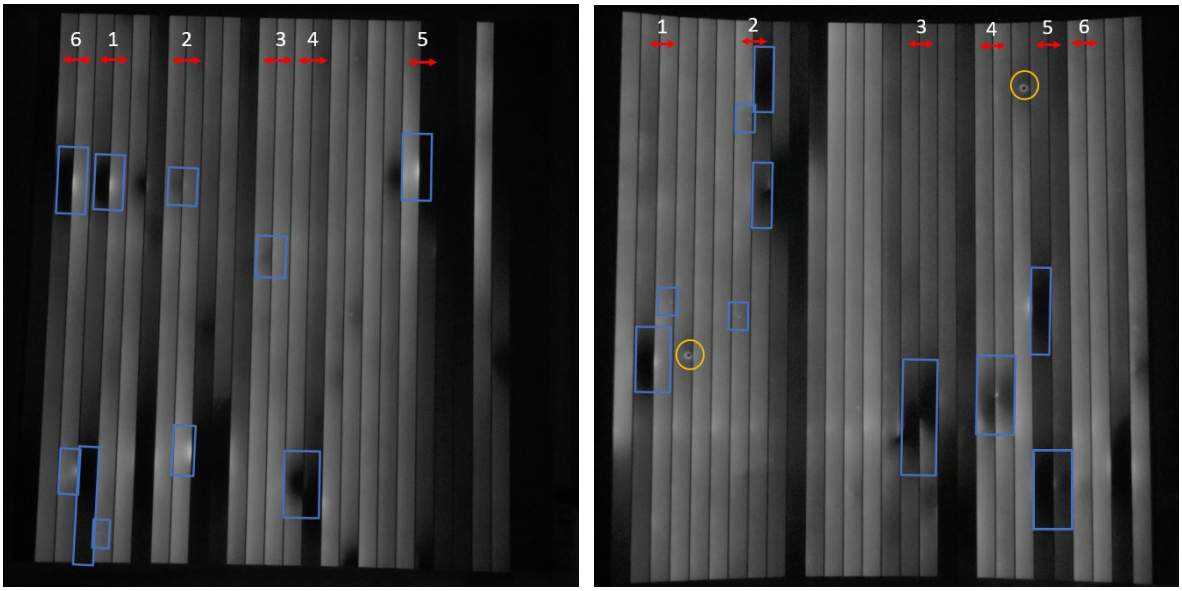

(a) R20026-4552 **(b)** R21020-3137

Figure 5.3: Represents the EL Images of R20026-4552 and R21020-3137 before light soaking the different pair of cells. The blue rectangles are defects that were found interesting to test on.

In the images above, the defects that were found interesting to test are marked by a blue rectangle. The reasons why the areas are chosen are:

- R20026-4552
    1. Current crowding at the top of the cell, white dot and half a cell is dark at the bottom
    2. Current crowding at the top and bottom of the cell
    3. Current crowding in the middle
    4. Dark region at the bottom
    5. Current crowding at the top
    6. Current crowding at the top and bottom
- R21020-3137
    1. Current crowing & dark region and white dot in the middle
    2. White dot and two dark regions at the top of the cell and a white dot in the middle
    3. Dark regions at the bottom
    4. Dark regions and a white dot in between them in the middle of the cell
    5. Dark region in the middle and a dark region + current crowding at the bottom, also the darkest pair of cells in the module
    6. No defects, but this pair is the brightest in the module

The pairs of cells are individually shadowed for each module in the order from area 1 to 6 for an hour at SC conditions in the light soaking machine that is available at the TU Delft. The results of the first round can be seen in the figures below.

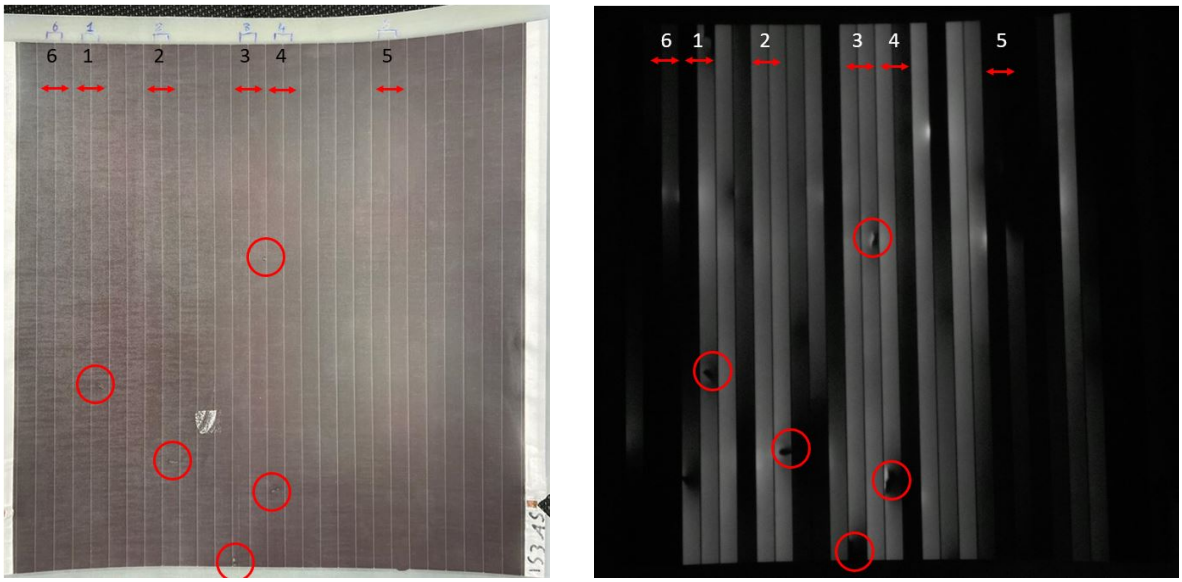

(a) Photograph after visual inspection **(b)** EL Images

Figure 5.4: Photograph after visual inspection and EL images of R20026-4552 right after the first round of light soaking

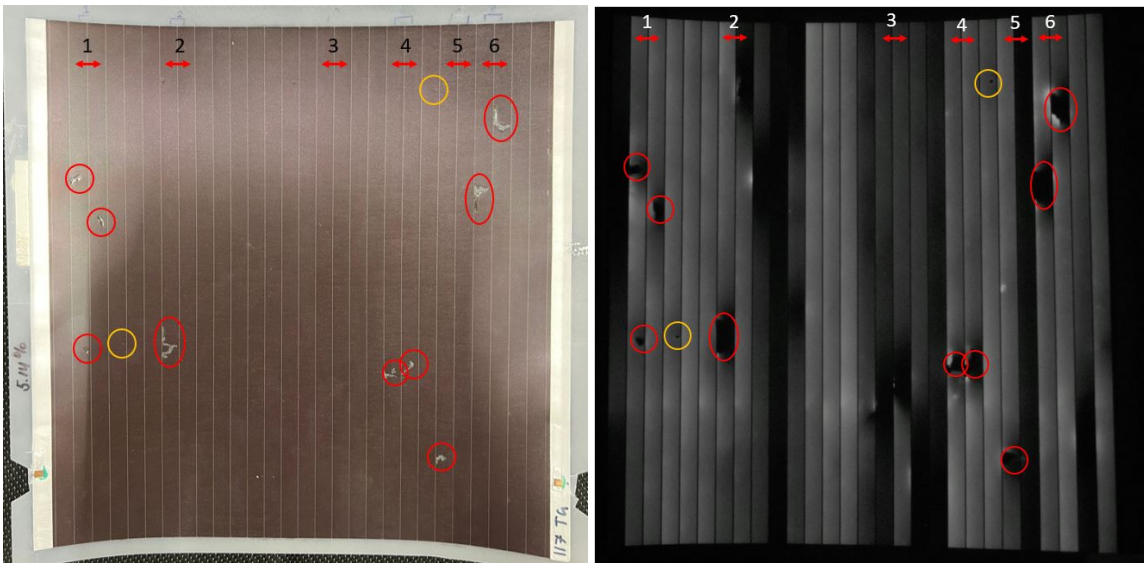

(a) Photograph after visual inspection **(b)** EL Images

Figure 5.5: Photograph after visual inspection and EL images of R21020-3137 right after the first round of light soaking

As seen in Figures 5.4 and 5.5, hotspots have formed in almost every area, except areas 5 and 6 of R20026-4552 and area 3 of R21020-3137. Furthermore, it is observed that some of these hotspots are larger when compared to the hotspots discussed in the previous chapter. IR imaging also gives interesting information: most hotspots did form just after five minutes of being in the light soaking machine and the temperature of the hotspots can range from 80-110°C. Figure 5.6 represents five IR images taken during light soaking. All hotspots that have formed had high temperatures in the IR images, reaching up to 95°C. Notice that these spots were already visible after 5 minutes of light soaking, as indicated by Figures 5.6a and 5.6c, indicating that these hotspots were already formed within these 5 minutes. Interesting to see is Figure 5.6e, which shows the IR image of Area 3 of R21020-3137 being shadowed after 1 hour. Although you can see a spot with an elevated temperature at the bottom of the area (the same spot marked in Figure 5.3b), no hotspots were formed. This might be because the temperature is too low in order to create the hotspots. All IR images of this procedure

can be found in Appendix A.2.

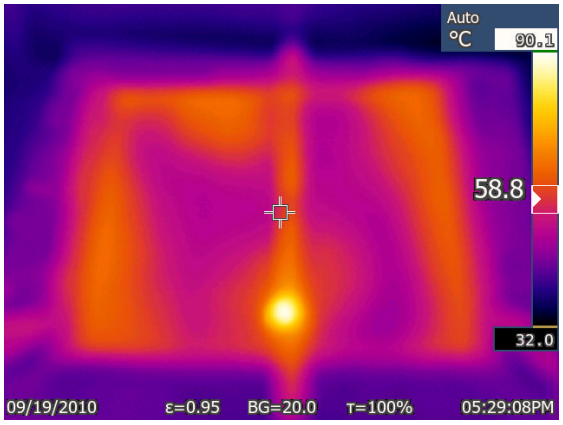

(a) Shading Area 4 of R20026-4552; image taken after 5 minutes

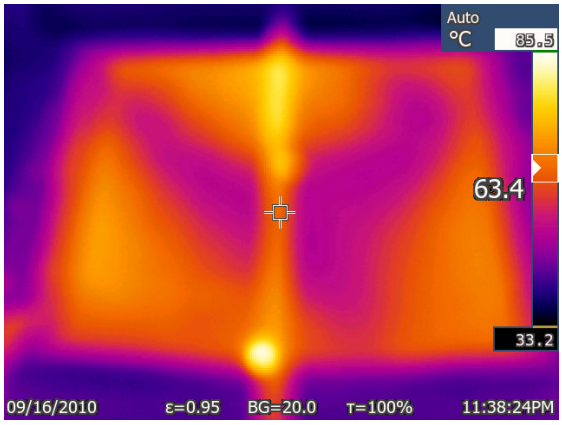

(b) Shading Area 3 of R20026-4552; image taken after 1 hour

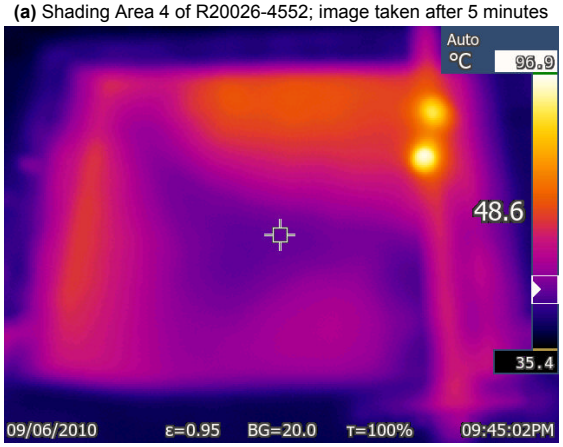

(c) Shading Area 6 of R21020-3137; image taken after 5 minutes

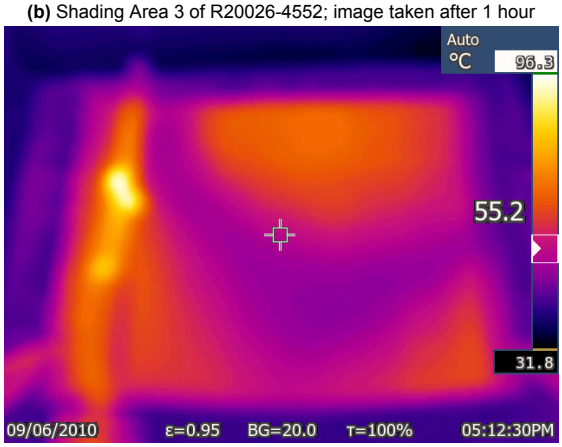

(d) Shading Area 1 of R21020-3137; image taken after 1 hour

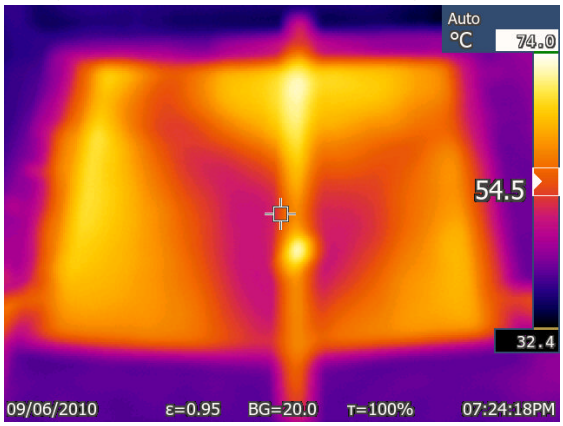

(e) Shading Area 3 of R21020-3137; image taken after 1 hour

Figure 5.6: IR Images taken after either 5 minutes or 1 hour during light soaking using the light soaking machine at the TU Delft

5.2.2. Second round

In order to get more data points, a second round of light soaking was carried out on the same modules by selecting additional areas of two and three for R20026-4552 and R21020-3137 respectively. These areas are marked in the images in Figure 5.7.

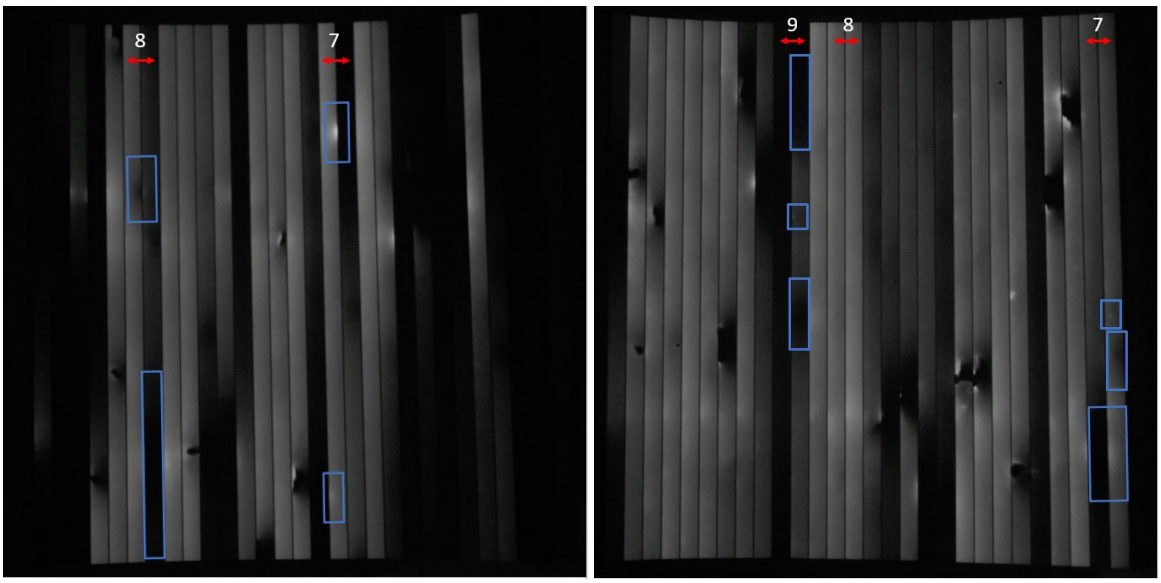

(a) R20026-4552 **(b)** R21020-3137

Figure 5.7: EL Images of R20026-4552 and R21020-3137 before the second round of light soaking and the areas that will be shaded are marked with numbers 7 and 8 in R20026-4552 and 7, 8 and 9 in R21020-3137

As with the first round, interesting defects are marked by a blue rectangle. The reasons why these extra areas were chosen are:

- R20026-4552

  7. Current crowding at the top and bottom and one cell is half dark
  8. Dark regions at the top and bottom of the cell

- R21020-3137

  7. White dot and dark region in the middle and current crowding + dark region at the bottom of the cell
  8. No defects, it seems like the best working pair of cells in the module
  9. Dark region at the top of the cell and a white dot and a dark region in the middle

Just like the first round, the areas get shadowed individually for an hour, which produced the following images in Figure 5.8 and 5.9.

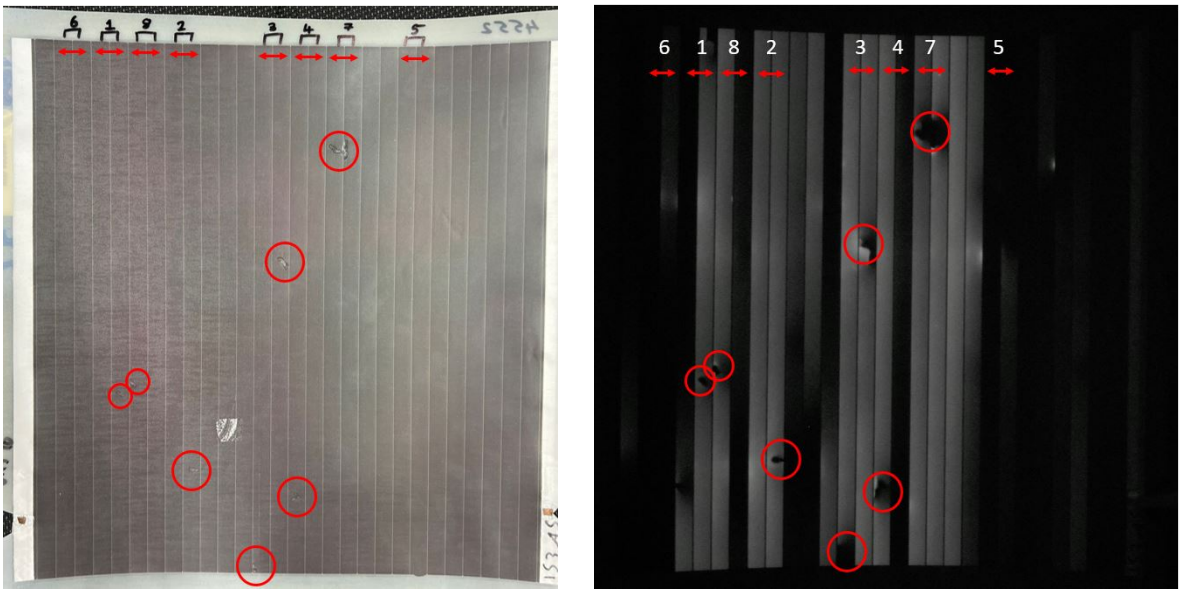

(a) Photograph after visual inspection **(b)** EL Images

Figure 5.8: Photograph after visual inspection and EL images of R20026-4552 right after the second round of light soaking

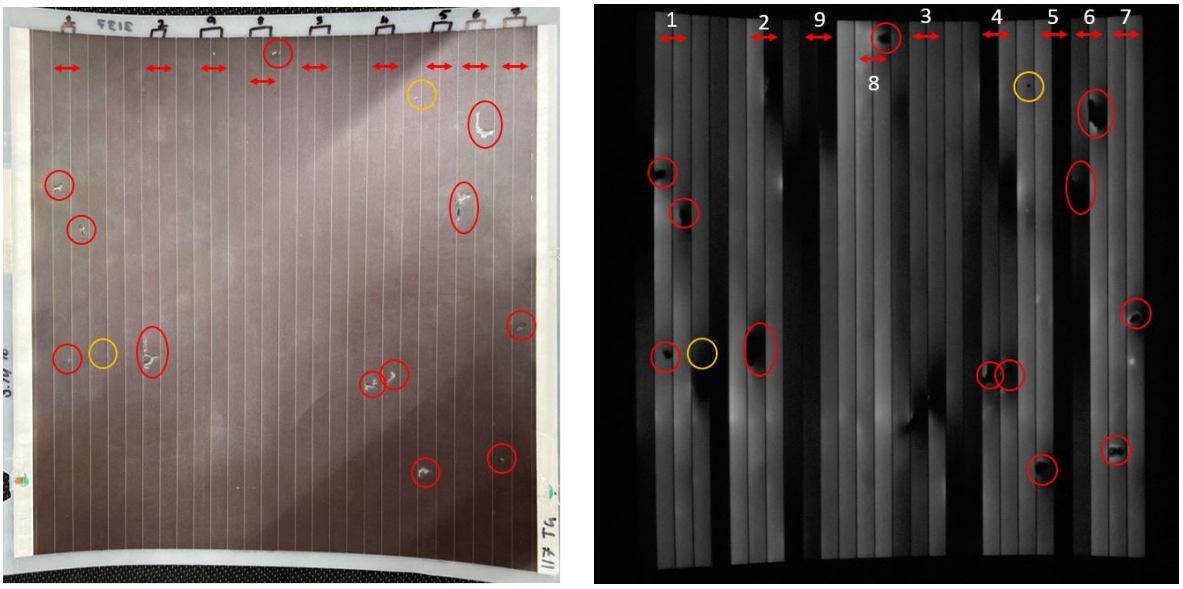

(a) Photograph after visual inspection **(b)** EL Images

Figure 5.9: Photograph after visual inspection and EL images of R21020-3137 right after the second round of light soaking

Figure 5.8 shows that two additional hotspots have formed during this round and Figure 5.9 three additional hotspots. For R20026-4552, one of the two hotspots came from current crowding, while the other had no predictor defect. One hotspot from R21020-3137 also had no predictor defect, while the other two came from current crowding and from a white dot. These hotspots also appeared to be bigger in size when compared to the hotspots created in Chapter 4. Additionally, both EL images are overall darker when compared to the EL images before the first round, which shows the degradation of the module.

5.3. Probability map

Figure 5.10 shows the probability map with the number of predictor defects and the corresponding numbers of hotspots formed from those predictors. The left graph is based on the modules R20026-4552 and R21020-3137 alone, whereas the right graph includes all four modules discussed so far. White dots have the highest probability of turning into hotspots, being 66.7% of the time on the left graph and 46.4% on the right; so almost half of the time that a white dot is being shadowed, it has turned turn into a hotspot. Current crowding has the lowest conversion probability, being 17.4% and 16.7% for the left and right graphs respectively. Dark regions fall in between the two, having a probability of 32.6% for the left graph and 32% for the right.

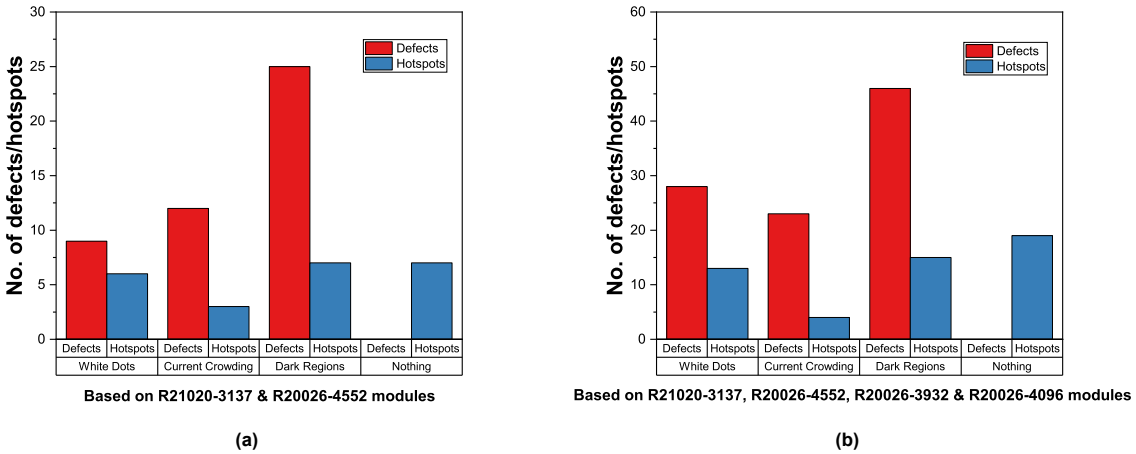

Figure 5.10: Probability Map of three different kinds of defects turning into hotspots

6

Classification and quantitative analyses of hotspots

This chapter focuses on the hotspots themselves; what kind of hotspots there are, the location of the hotspots and when they were created. Furthermore, the relation between defects and the interconnection of cells is also investigated.

6.1. Classification of hotspots based on shape

Just as the classification for defects in the EL images, a classification was also made for the resulting hotspots, which can be seen in Figure A.4. The image on the left shows a hotspot in the form of a circle, hence classified as a 'circular' hotspot. The middle image shows a 'linear' hotspot; this hotspot can either be a horizontal or vertical line. It is also noticed that the linear hotspot can be inclined at 45° as well (refer the high magnification images in Appendix A.1). The last hotspot is classified as 'linear along the scribe', which is a vertical hotspot that is present along the scribe between two cells.

Figure 6.1: Classification of three different hotspots present on the modules. The left image is a 'circular' hotspot, the middle image is a 'linear' hotspot and the right image is a 'linear along the scribe' hotspot.

All the defects and hotspots created have been visualized in a graph in Figure 6.2a. White dots will turn primarily into circular hotspots, while dark region defects will turn into linear hotspots most of the time. Current crowding will lead to circular or linear hotspots most of the time. It was expected that this defect would turn into linear along the scribe hotspots, as it is present at the scribe of a cell. Hotspots that did not have a predictor defect have an equal chance of being one of the three classified hotspots.

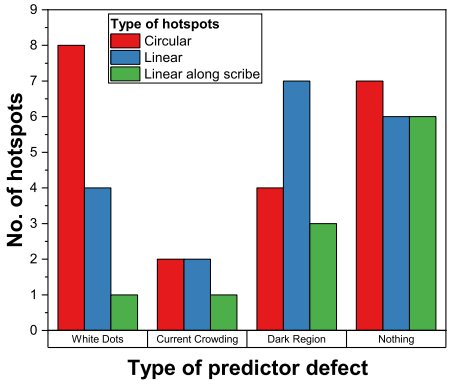

(a) The number of certain types of hotspots that were created by which defect

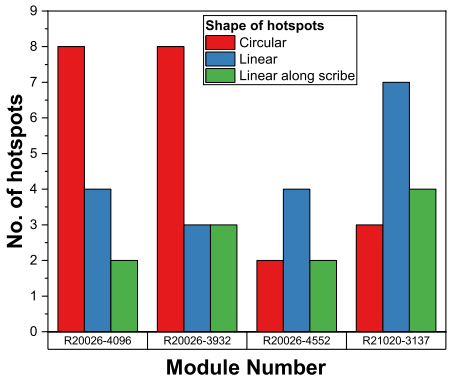

(b) The number of certain types of hotspots per solar module

Figure 6.2: Visualization of the types of hotspots against the modules and what kind of defects it originated from

Figure 6.2b shows that modules R20026-4096 and R20026-3932 both have a high number of circular hotspots, far more than linear and linear along the scribe. Note that the modules R20026-4552 and R21020-3137 both have an increased number of linear hotspots, more than circular and linear along the scribe hotspots. The difference here lies in the time that the module is getting light soaked for: most of the circular hotspots created in the first pair of modules were the result of doing the WSS procedure. Here, the cells are being shaded for less than a minute instead of an hour. The circular hotspots are further light soaked for 1 hour to see their growth and the results are shown in Figure 6.3. The circular hotspots that were caused by WSS now all expanded into bigger hotspots that can be classified as linear hotspots. So, if a hotspot is shadowed long enough, it will turn into a linear hotspot and if not, it will remain a circular one.

(a) Before

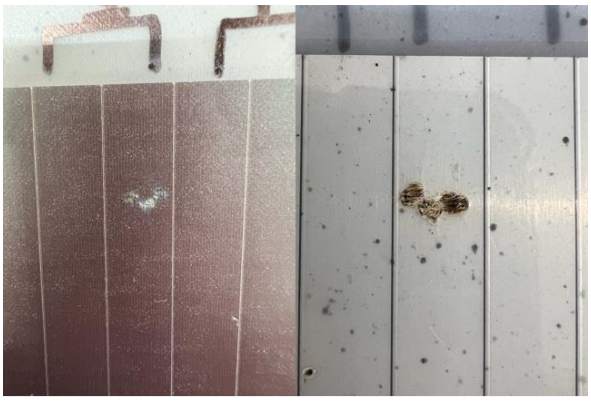

(b) After

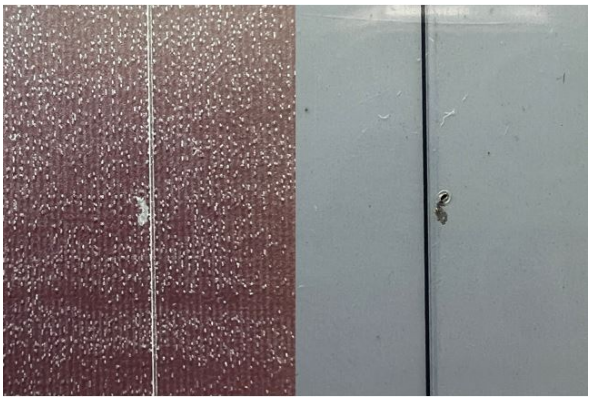

(c) Before

(d) After

(e) Before **(f)** After

(g) Before **(h)** After

Figure 6.3: Already existing hotspots getting larger after getting shadowed and light soaked at SC conditions for 1 hour

6.2. Classification of hotspots based on location

In order to see if location plays a role in the creation of hotspots, the X and Y-location of the hotspots have to be determined. The solar module has to be placed so that the contact points are at the bottom (Figure 6.4a). For the X-location, it is divided into three equal sections of 1/3 of the cell width: left, middle and right as indicated in Figure 6.4b. For the Y-location, the whole module (hence each cell) is divided into three equal sections as well, but now in the vertical direction; top, middle and bottom, as seen in Figure 6.5.

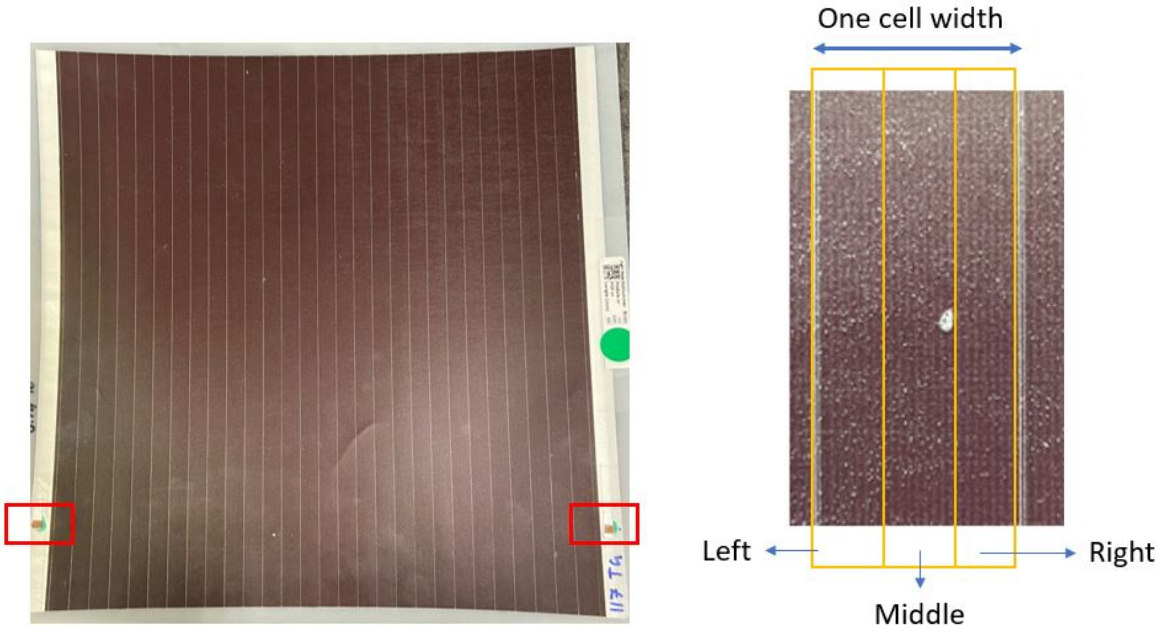

(a) (b)

Figure 6.4: Classification of the X-location of hotspots; the module has to be placed in a way such that the contact points (red rectangles) are at the bottom

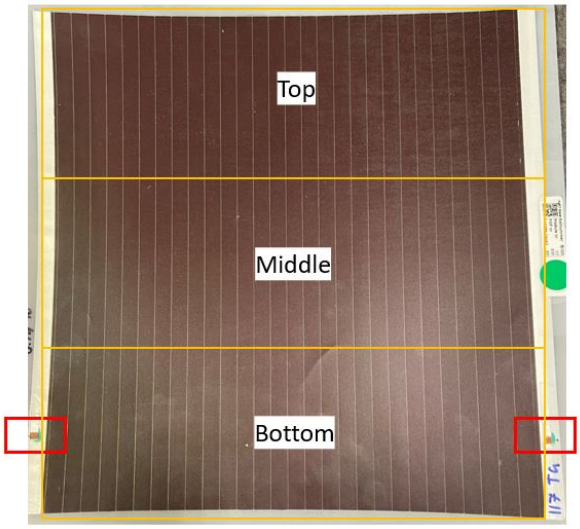

Figure 6.5: Classification of the Y-location of hotspots; the module has to be placed in a way such that the contact points (red rectangles) are at the bottom

From Figure 6.6a, it can be seen that R20026-4096 and R20026-3932 have a majority of their hotspots at either the left or right side of the cell. This can be accounted for by the presence of more circular hotspots. The other way around is true for the other two modules; more hotspots present in the middle of the cell and fewer hotspots at either side. This can be correlated to the presence of more linear hotspots. As expected linear along the scribe hotspots are almost always on the left scribe of the cell. The direction of growth of linear along the scribe was always parallel to the scribe lines. This analysis along with Figure 6.6a, suggest that white dot related defects are bulk defects and can be present everywhere in the module.

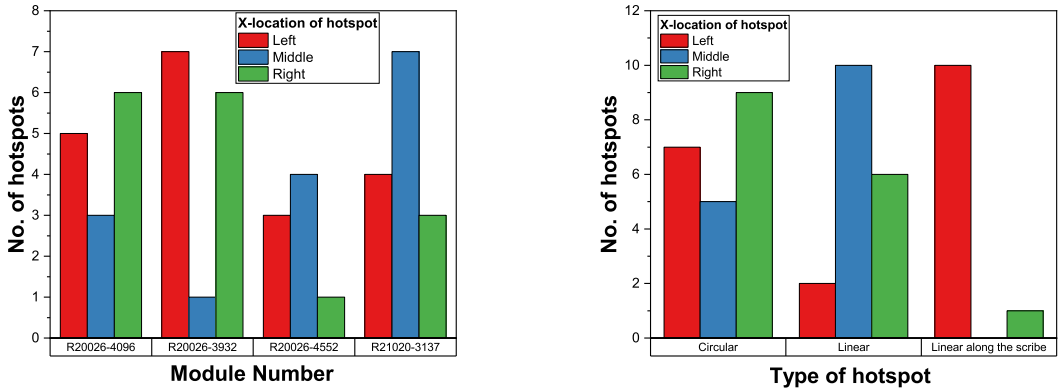

(a) X-Location and module of the hotspots

(b) X-location and the types of hotspots

Figure 6.6: The X-locations of the hotspots per module and per type of hotspots

For Y-location, R20026-4096 and R20026-3932 show similar trends with most hotspots located at either the bottom or top of the module, as can be seen in Figure 6.7. Looking at the other two modules, no correlation can be found. The same goes for the location and the type of hotspot. Circular hotspots are nearly uniformly distributed, as well as linear along the scribe hotspots. Linear hotspots seem to form mainly at the top and bottom of the modules.

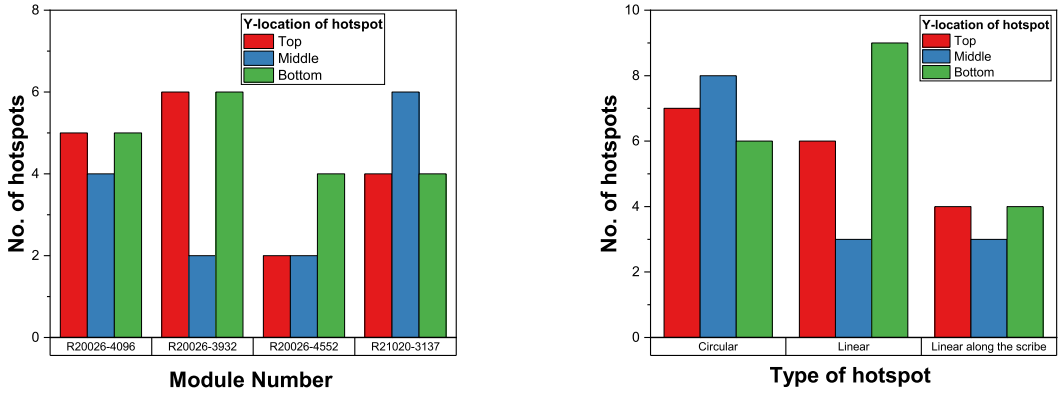

(a) Y-Location and module of the hotspots

(b) Y-location and the types of hotspots

Figure 6.7: The Y-locations of the hotspots per module and per type of hotspots

6.3. Cause of defects

It is also important to find out where these defects originated from. White dots are defects that show up as little dots that are brighter than the surrounding solar cell. They are expected to be a manufacturing process flaw; a high concentration of a certain type of material can cause a white dot, as well as sharp tips in the substrates. Current crowding and dark regions always come in pairs. Figure 2.5 shows the interconnection between cells in the modules from HyET and is used to better understand how these defects can occur. If current crowding is seen on the left scribe of the cell, it is suspected that something is wrong with the P2s. If the P2s is faulty, the current flow experiences higher resistance and can cause the current to accumulate at one location, which would result in brighter spots present in EL images. This would also explain why there would be a black region in the previous cell. Now, if the current crowding is on the right side of the scribe, it is suspected that the P3 causes this defect. If the P3 is faulty, the back contacts might be connected, short-circuiting the cell and making an area of the cell or the whole cell dark. This would explain why the cell adjacent to the right of the current crowding would be dark.

7

Conclusion

The purpose of this thesis was to gain insights into a deeper understanding of hotpot formation in thin-film a-Si modules in accordance to the latest IEC 61216 certification norms. To do so, several advanced characterization techniques were used like EL and IR imaging, as well as the LASS and light soaking machines at HyET and the TU Delft.

After following the IEC 61215 certification norms, multiple hotspots can be found on the highly degraded modules used for this procedure. Most of these hotspots had a predictor defect present in EL images before being formed. This means that EL imaging is a good tool for finding defects in thin-film a-Si modules that possibly can turn into hotspots. Also, it became apparent that some of the hotspots were created during the WCSS procedure.

The defects found in EL imaging can be one of three kinds of defects: current crowding, white dots and dark regions. It was observed that current crowding is always paired with dark regions. If current crowding is present near the left scribe of a cell, a dark region is present in the previous cell, and if current crowding is present near the right scribe of a cell, a dark region can be found in the next cell. The reason for this is probably a scribing issue in the cells. White dots have the highest probability of causing hotspots, being 46.4%. Following is dark regions with 32% and current crowding has the least probability of causing hotspots, which being 16.7%. Also, the IR images indicate that hotspots can already be seen with elevated temperatures after just 5 minutes. This, in combination with the hotspots formed during the WCSS, shows that hotspots can be formed quickly while being shadowed during light soaking at SC conditions.

To see what would happen to the hotspots created during the WCSS when light soaked for extended periods of time, these hotspots were shadowed for 1 hour. Ultimately, the circular hotspots turned into linear hotpots during this process. Linear hotspots are always either perpendicular or at an angle of 45°. Hotspots that were classified as 'linear along the scribe' originated largely from either dark regions or did not have a predictor defect present. Furthermore, white dots are likely to produce circular hotspots and dark regions will mainly result in linear hotspots.

Although no thorough analysis is done on the origin of the defects, there are some thoughts on what might be the cause of them. For white dots, it is expected to be a manufacturing process flaw. A high concentration of a certain type of material can cause a white dot to appear, but also sharp tips in the carrier foil. Current crowding and dark regions are probable scribe issues. If current crowding is visible on the left side of a cell, there is probably something wrong with the P2 scribe, and if it appears on the right side of the cell, this can be accounted to the P3 scribe.

For further work, it is recommended to investigate the interconnection between cells, with a focus on the P2 and P3 scribes and improve them if needed, as those might be the culprit of the current crowding and dark region defects. Also, see if different settings on the camera or a different lens can influence the EL images. Now, some hotspots were created without any predictor defects present in these images, but maybe with different camera settings, these might appear and give more insights into the thin-film a-Si modules. In this regard, thermal imaging-based characterization of shunts might be a better defect predictor technique. Further, investigate the reverse bias characteristics of each cell

individually and see if there is any correlation with hotspot formation. Next, study the role of aging of thin-film a-Si in hotspot formation. And lastly, repeat the analysis done on no degraded/new modules and on modules with different sizes and dimensions, as that might bring some new interesting insights into hotspot formation in thin-film a-Si modules.

References

[1] I. E. Agency. “Solar pv.” (2023), [Online]. Available: https://www.iea.org/energy-system/renewables/solar-pv (visited on 11/09/2023).

[2] REGlobal. “Technology roadmap: Anticipated trends in the c-si pv industry.” (2022), [Online]. Available: https://reglobal.org/technology-roadmap-anticipated-trends-in-the-c-si-pv-industry/ (visited on 11/09/2023).

[3] S. Hansen. “Amorphous vs. crystalline: How to determine the best solar technology for your application.” (2023), [Online]. Available: https://blog.powerfilmsolar.com/education/the-horizon-blog/2019/01/28/amorphous-vs-crystalline-the-best-technology-for-your-application (visited on 11/09/2023).

[4] S. Wigness. “Solar panel warranty guide: What you need to know.” (2023), [Online]. Available: https://www.solar.com/learn/solar-panel-warranty-guide-what-you-need-to-know/.

[5] S. Voltaics. “Iec 61215 certification testing.” (n.a.), [Online]. Available: https://sinovoltaics.com/iec-61215-certification-testing/.

[6] M. Maghami, H. Hizam, C. Gomes, M. Radzi, M. Rezadad, and S. Hajighorbani, “Power loss due to soiling on solar panel: A review,” *Renewable and Sustainable Energy Reviews*, vol. 59, pp. 1307–1316, 2016, ISSN: 1364-0321. DOI: https://doi.org/10.1016/j.rser.2016.01.044. [Online]. Available: https://www.sciencedirect.com/science/article/pii/S1364032116000745.

[7] RenewSys. (2020), [Online]. Available: https://www.renewsysworld.com/post/when-solar-panels-are-put-on-a-hotspot (visited on 08/04/2023).

[8] P. Education. “Hotspot heating.” (n.a.), [Online]. Available: https://www.pveducation.org/pvcdrom/modules-and-arrays/hot-spot-heating (visited on 08/08/2023).

[9] REdeMexico, 2018. [Online]. Available: https://twitter.com/REdemexico/status/1051495585067528192 (visited on 08/08/2023).

[10] A. Smets. “Amorhpous silcon.” (2021), [Online]. Available: https://ocw.tudelft.nl/course-lectures/amorphous-silicon/ (visited on 08/08/2023).

[11] H. Kang, “Crystalline silicon vs. amorphous silicon: The significance of structural differences in photovoltaic applications,” *IOP Conference Series: Earth and Environmental Science*, vol. 726, no. 1, p. 012 001, Apr. 2021. DOI: 10.1088/1755-1315/726/1/012001. [Online]. Available: https://dx.doi.org/10.1088/1755-1315/726/1/012001.

[12] M. Simon and E. Meyer, “Detection and analysis of hot-spot formation in solar cells,” *Solar Energy Materials and Solar Cells*, vol. 94, no. 2, pp. 106–113, 2010, ISSN: 0927-0248. DOI: https://doi.org/10.1016/j.solmat.2009.09.016. [Online]. Available: https://www.sciencedirect.com/science/article/pii/S0927024809003420.

[13] P. Guerriero, P. Tricoli, and S. Daliento, “A bypass circuit for avoiding the hot spot in pv modules,” *Solar Energy*, vol. 181, pp. 430–438, 2019, ISSN: 0038-092X. DOI: https://doi.org/10.1016/j.solener.2019.02.010. [Online]. Available: https://www.sciencedirect.com/science/article/pii/S0038092X19301355.

[14] T. Weber, A. Albert, N. Ferretti, M. Roericht, S. Krauter, and P. Grunow, “Electroluminescence investigation on thin film modules,” Sep. 2011. DOI: 10.4229/26thEUPVSEC2011-3AV.1.50.

[15] R. Ebner, S. Zamini, and G. Újvári, “Defect analysis in different photovoltaic modules using electroluminescence (el) and infrared (ir)-thermography,” Jan. 2010, pp. 333–336. DOI: 10.4229/25thEUPVSEC2010-1DV.2.8.

[16] D. Matusz-Kalász and I. Bodnár, “Monitoring and diagnostics of photovoltaic cells by electroluminescence,” in *2022 23rd International Carpathian Control Conference (ICCC)*, 2022, pp. 158–161. DOI: 10.1109/ICCC54292.2022.9805888.

[17] E. Kaplani, “Degradation in field-aged crystalline silicon photovoltaic modules and diagnosis using electroluminescence imaging,” in *Proc. 8th International Workshop on Teaching in Photovoltaics (IWTPV'16)*, vol. 2016, Apr. 2016, pp. 38–41, ISBN: 978-80-01-05935-7. [Online]. Available: https://ueaeprints.uea.ac.uk/id/eprint/58215/.

[18] S. Gallardo-Saavedra, L. Hernández-Callejo, M. Alonso-García, *et al.*, “Nondestructive characterization of solar pv cells defects by means of electroluminescence, infrared thermography, i–v curves and visual tests: Experimental study and comparison,” *Energy*, vol. 205, p. 117 930, 2020, ISSN: 0360-5442. DOI: https://doi.org/10.1016/j.energy.2020.117930. [Online]. Available: https://www.sciencedirect.com/science/article/pii/S0360544220310379.

[19] S. Ahsan, K. Niazi, H. Khan, and Y. Yang, “Hotspots and performance evaluation of crystalline-silicon and thin-film photovoltaic modules,” *Microelectronics Reliability*, vol. 88-90, pp. 1014–1018, 2018, 29th European Symposium on Reliability of Electron Devices, Failure Physics and Analysis (ESREF 2018), ISSN: 0026-2714. DOI: https://doi.org/10.1016/j.microrel.2018.06.097. [Online]. Available: https://www.sciencedirect.com/science/article/pii/S0026271418305171.

[20] Newport. “Solar simulator standards – definitions comparisons.” (2023), [Online]. Available: https://www.newport.com/n/solar-simulator-standards-definitions-and-comparisons (visited on 08/07/2023).

[21] Biophlox. (2023), [Online]. Available: https://www.biophlox.com/lab-equipment/general-lab-equipment/lab-others/Fluke-TI32-Thermal-Imaging-Infrared-Camera-T-132 (visited on 08/04/2023).

[22] Meetwinkel. (2023), [Online]. Available: https://meetwinkel.nl/p/fluke-568-ir-en-contact-thermometer/ (visited on 08/04/2023).

A

Images

A.1. High resolution visual images

Figure A.1: High resolution visual images of the hotspots of R20026-4096

Figure A.2: High resolution visual images of the hotspots of R20026-3932

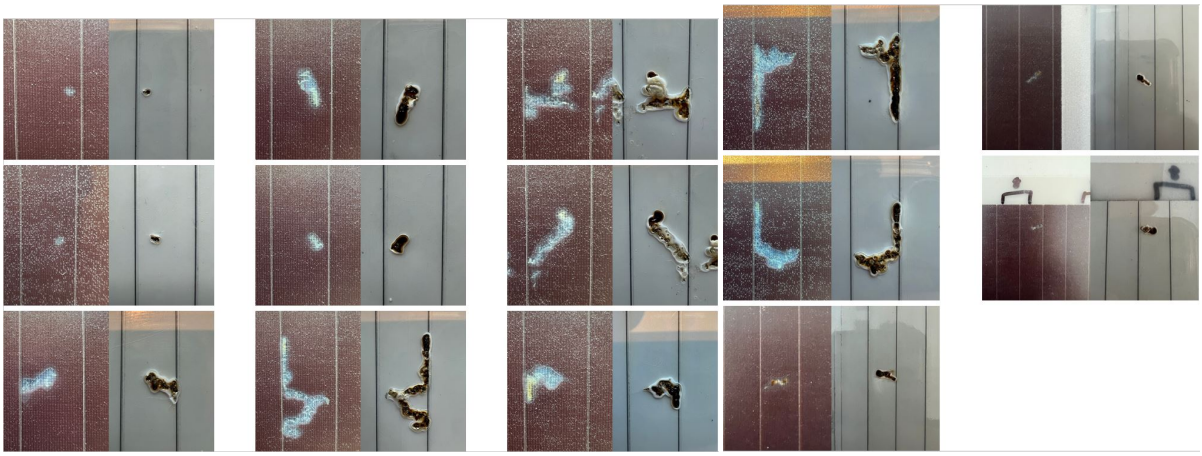

Figure A.3: High resolution visual images of the hotspots of R21020-3137

Figure A.4: High resolution visual images of the hotspots of R20026-4552

A.2. IR images

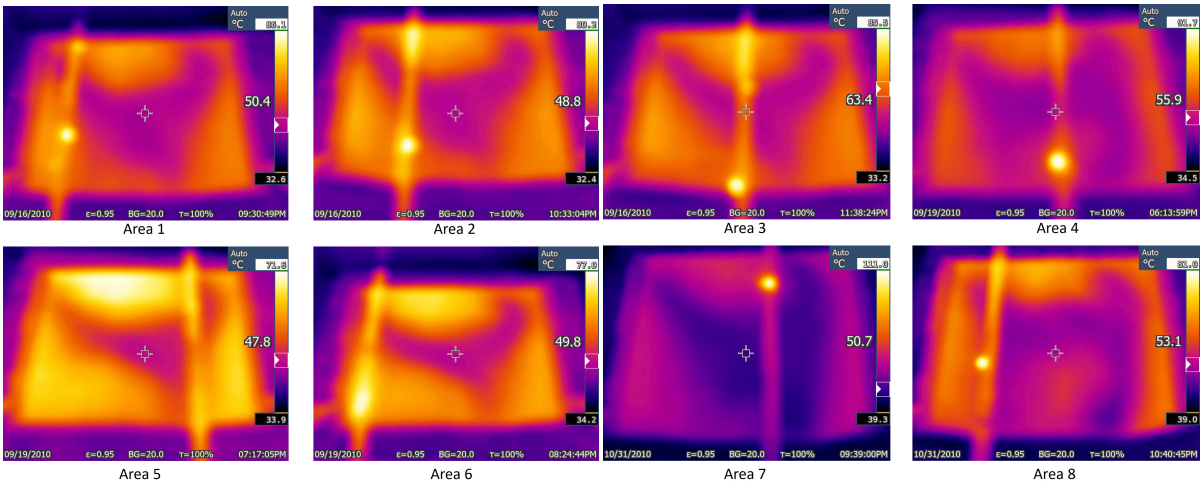

Figure A.5: Represents all the IR images of the different shadowed areas after an hour of light soaking of R20026-4552

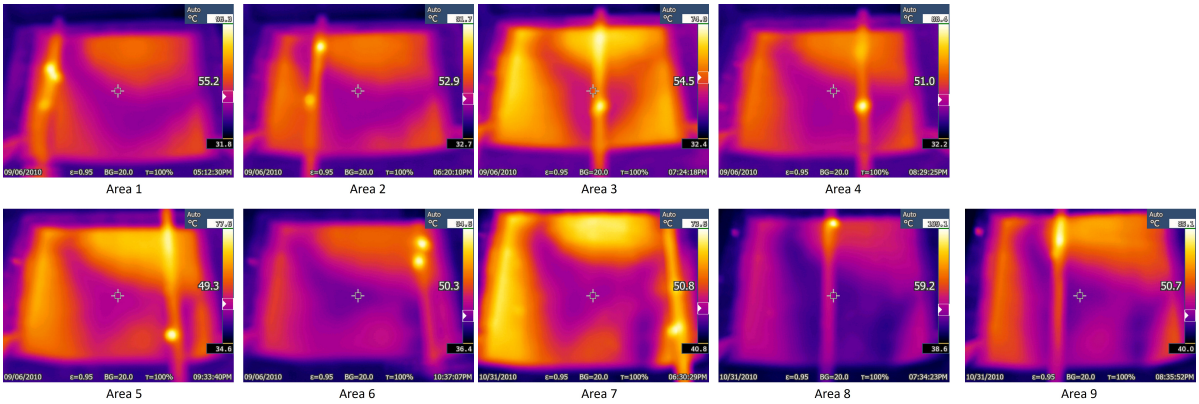

Figure A.6: Represents all the IR images of the different shadowed areas after an hour of light soaking of R21020-3137

B

Datasheets

B.1. Nikon D7200 camera

Nikon

At the heart of the image™

D7200 & D7100
COMPARISON SHEET

D7200™

I AM CHALLENGE READY

D7100™

I AM 24 MP UNLEASHED

SENSOR AND RESOLUTION		
Sensor	23.5 x 15.6mm	23.5 x 15.6mm
Resolution	24.2 DX-format CMOS sensor without an Optical Low Pass Filter (OLPF)	24.1 DX-format CMOS sensor without an Optical Low Pass Filter (OLPF)
IMAGE QUALITY		
Image Processing Engine	EXPEED 4*	EXPEED 3
ISO Sensitivity Range	ISO 100 to 25,600 Hi BW1 (51,200), Hi BW2 (102,400)	100-6,400 up to Hi2 (ISO 25,600)
File Format	12-bit and 14-bit NEF (RAW) File support JPEG- fine (approx. 1: 4), normal (approx. 1: 8), basic (approx. 1: 16) TIFF (RGB)	12-bit and 14-bit NEF (RAW) File support JPEG- fine (approx. 1: 4), normal (approx. 1: 8), basic (approx. 1: 16) TIFF (RGB)
Picture Control	Standard, Neutral, Vivid, Portrait, Landscape • New Flat Picture Control: Ideal for Video Capture • New Clarity Control: Ideal for adding Definition • Finer control with 0.25-step adjustment	Standard, Neutral, Vivid, Portrait and Landscape
METERING SYSTEM		
3D Color Matrix Metering II (2016k RGB Sensor)	Yes	Yes
Scene Recognition System	Yes	Yes
WHITE BALANCE		
Spot White Balance when using Live View	Yes	Yes
Preset Manual White Balance	1-6 possible	1-3 is possible
AUTO FOCUS		
AF Sensor	Advanced Multi-CAM 3500 II DX AF detection range down to -3 EV, 51 focus points (15 cross-type sensors in the center, one point compatible with f/8) Live view photography (stills/movies): contrast-detect AF	Advanced Multi–CAM 3500 DX AF detection range down to -2 EV, 51 focus points (15 cross-type sensors in the center, one point compatible with f/8) Live view photography (stills/movies): contrast-detect AF
Dynamic AF Modes	9/21/51, 51 points w/3D Tracking, Auto Area AF	9/21/51, 51 points w/3D Tracking, Auto Area AF
Separate selection of both focus point and AF-area mode for landscape and portrait orientation	Yes	No
RELEASE MODES		
Frame Advance Rate	6 fps in DX, 7 fps in 1.3X Crop Mode	6 fps in DX, 7 fps in 1.3X Crop Mode
Buffer Capacity (With 16GB Class 10 SD Card)	• NEF (RAW), Lossless Compressed, 12-bit: 27 Shots • NEF (RAW)), Lossless Compressed 14-bit: 18 Shots • JPEG/Fine/Large: 100 shots	• NEF (RAW), Lossless Compressed, 12-bit: 7 Shots • NEF (RAW)), Lossless Compressed 14-bit: 6 Shots • JPEG/Fine/Large: 33 shots
CONNECTIVITY		
Wi-Fi Connectivity	Built-in Wi-Fi with NFC (Near Field Communication)	Uses WU-1a Wireless Mobile Adapter (Optional)

**EXPEED 4 benefits: 30% faster than EXPEED 3, increased number of continuous shots, improved Noise Reduction, improved White Balance, enhanced definition: Clarity Picture Control, 1080 @60p (1.3X Crop Mode)*

Specifications are subject to change without notice.

D7200 & D7100
COMPARISON SHEET

At the heart of the image™

D7200™

I AM CHALLENGE READY

D7100™

I AM 24 MP UNLEASHED

	D7200	D7100
VIDEO		
Frame Size and Frame rate	1920 x 1080 30/25/24p 1920 x 1080 60/50p (1.3X Crop)	1920 x 1080 30/25/24p 1920 x 1080 60i (1.3X Crop Mode)
ISO Range	ISO 100 to 25,600	ISO 100 to 6,400
Picture Control	Standard, Neutral, Vivid, Portrait, Landscape • New Flat Picture Control: Ideal for Video Capture • Finer control with 0.25-step adjustment	Standard, Neutral, Vivid, Portrait and Landscape
Selectable Audio Frequency Range	Yes Wide/Voice	Yes
Interval Timer Exposure Smoothing	Yes	Interval Timer Only
Time-Lapse Exposure Smoothing	Yes	No
Number or intervals in Time-lapse/Interval Timer Sequences	Up to 9,999	Up to 999
Auto ISO in Manual Mode	Yes	No
Dedicated Movie Menu	Yes	No
Highlight Display (Zebra Stripes) in Live View	Yes	No
Simultaneous display of videos on the LCD monitor and an external monitor	Yes	Yes
Built-in Stereo Microphone	Yes	Yes
OTHER FEATURES		
LCD Size and Resolution	3.2 inch, Approx. 1,229k-Dot with RGBW Alignment	3.2 inch, Approx. 1,229k-Dot with RGBW Alignment
Optical Viewfinder	• Optical viewfinder with approx. 100% frame coverage • Improved coatings on optical glass render brighter and more accurate color • Organic EL Information display makes it easier to make adjustments under bright/dim conditions	• Optical viewfinder with approx. 100% frame coverage • Organic EL Information display makes it easier to make adjustments under bright/dim conditions
Dual SD Card Slots	Yes	Yes
Dedicated Photo Shooting Menu	Yes	No
Auto Bracketing	1-9 frames	1-5 frames
Software for browsing and developing NEF (RAW)	View NX-i (Browsing), View NX-D (Developing) Available via free download	View NX-2, Capture NX-2
Battery Performance	1110 shots (Based on CIPA standards) 80 minutes of video (Based on CIPA standards	950 shots (Based on CIPA standards) 100 minutes of video (Based on CIPA standards
Dimensions (W x H x D)	Approx. 5.3 x 4.2 x 3.0 in. (135.5 x 106.5 x 76mm)	Approx. 5.3 x 4.2 x 3.0 in. (135.5 x 106.5 x 76mm)
Weight	Approx. 765 g (1 lb 11.0 oz)	Approx. 765 g (1 lb 11.0 oz)

Wi-Fi® COMPATIBILITY: *Nikon Cameras having built-in Wi-Fi capability or connected to a WU-1a or WU-1b Wireless Mobile Adapter can only be used with a compatible iPhone®, iPad®, and/or iPod touch® or smart devices running on the Android™ operating system.*

NFC (near field communication) Compatibility: *Nikon Cameras having built-in NFC capability can only be used with a compatible smart devices running on the Android™ operating system version 4.0 or higher.*

Nikon Wireless Mobile Utility application. The Nikon Wireless Mobile Utility application must be installed on the device before it can be used with cameras having built-in Wi-Fi and/or NFC capability or connected to a WU-1a or WU-1b Wireless Mobile Adapter.

Android and Google Play are trademarks of Google Inc. Wi-Fi® and the Wi-Fi CERTIFIED logo are registered trademarks of the Wi-Fi Alliance. The N Mark is a trademark or registered trademark of NFC Forum, Inc. in the United States and in other countries. All Nikon trademarks are trademarks of Nikon Corporation.

Specifications are subject to change without notice.

B.2. AF-S NIKKOR 28mm f/1.8G lens

For Your Safety

⚠ CAUTIONS

- **Do not disassemble**. Touching the internal parts of the camera or lens could result in injury. In the event of malfunction, the product should be repaired only by a qualified technician. Should the product break open as the result of a fall or other accident, remove the camera battery and/or disconnect the AC adapter and then take the product to a Nikon-authorized service center for inspection.
- **Turn the camera off immediately in the event of malfunction**. Should you notice smoke or an unusual smell coming from the equipment, immediately unplug the AC adapter and remove the camera battery, taking care to avoid burns. Continued operation could result in fire or injury. After removing the battery, take the equipment to a Nikon authorized service center for inspection.
- **Do not use in the presence of flammable gas**. Operating electronic equipment in the presence of flammable gas could result in explosion or fire.
- **Do not look at the sun through the lens or the camera viewfinder**. Viewing the sun or other bright light source through the lens or viewfinder could cause permanent visual impairment.
- **Keep out of reach of children**. Failure to observe this precaution could result in injury.
- **Observe the following precautions when handling the lens and camera**:
  - Keep the lens and camera dry. Failure to observe this precaution could result in fire or electric shock.
  - Do not handle the lens or camera with wet hands. Failure to observe this precaution could result in electric shock.
  - Keep the sun well out of the frame when shooting backlit subjects. Sunlight focused into the camera when the sun is in or close to the frame could cause a fire.
  - If the lens will not be used for an extended period, attach the front and rear lens caps and store the lens out of direct sunlight. If left in direct sunlight, the lens could focus the sun's rays onto flammable objects, causing fire.
- **Do not carry tripods with a lens or camera attached**. You could trip or accidentally strike others, resulting in injury.
- **Do not leave the lens where it will be exposed to extremely high temperatures, such as in an enclosed automobile or in direct sunlight**. Failure to observe this precaution could adversely affect the lens' internal parts, causing fire.

Notice for Customers in Canada

CAN ICES-3 B / NMB-3 B

Thank you for your purchase of an AF-S NIKKOR 28mm f/1.8G lens. Before using this product, please carefully read both these instructions and the camera manual.

Note: When mounted on a DX-format digital single-lens reflex camera such as the D7000 or cameras in the D300 series, this lens has an angle of view of 53° and a focal length equivalent to 42 mm (35 mm format).

■ Parts of the Lens

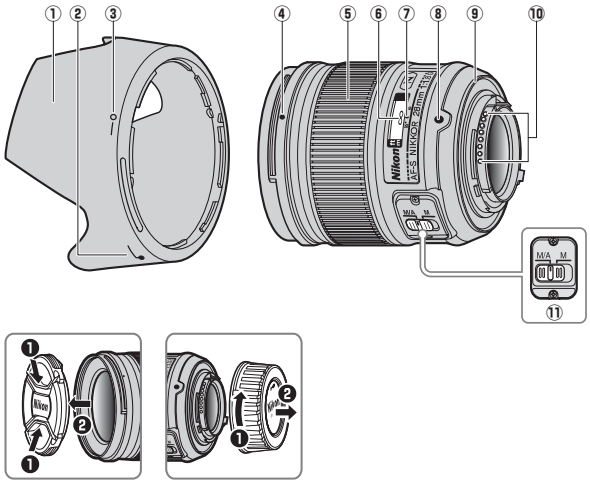

① Lens hood 16
② Lens hood alignment mark 16
③ Lens hood lock mark 16
④ Lens hood mounting mark 16
⑤ Focus ring 15
⑥ Focus distance indicator ... 16
⑦ Focus distance mark 16
⑧ Lens mounting mark
⑨ Rubber lens-mount gasket 18
⑩ CPU contacts 18
⑪ Focus-mode switch 15

■ Compatibility

Check marks ("✔") indicate supported features, dashes ("—") features that are not supported. Some limitations may apply; see the camera manual for details.

Camera	Exposure (Shooting) mode				AF[5]
	P[4]	S	A	M	
Nikon FX-format and DX-format digital single-lens reflex cameras	✔	✔	✔	✔	✔
F6, F5, F100, F/N80-series[1], F/N75-series[1], F/N65-series[1], Pronea 600i/6i[1], Pronea S[2]	✔	✔	✔	✔	✔
F4-series, F90X/N90s[1], F90-series/N90[1], F70-series/N70[1]	✔	✔	—	—	✔
F60-series/N60[1], F/N55-series[1], F50-series/N50[1], F-401x/N5005[1], F-401s/N4004s[1], F-401/N4004[1]	✔	✔	✔	✔	—
F-801s/N8008s[1], F-801/N8008[1], F-601M/N6000[1]	✔	✔	—	—	—
F3AF, F-601/N6006[1], F-501/N2020[3], Nikon manual focus cameras (excluding F-601M/N6000[1])	—				

1 N-series cameras and Pronea 6i sold in U. S. A. only.
2 Exposure mode M (manual) not available.
3 N2020 sold in U. S. A. and Canada only.
4 Includes AUTO and scene (Digital Vari-Program) modes.
5 Autofocus.

■ Focus

Supported focus modes are shown in the following table (for information on camera focus modes, see the camera manual).

Camera	Camera focus mode	Lens focus mode	
		M/A	M
Nikon FX-format and DX-format digital single-lens reflex cameras, F6, F5, F4-series, F100, F90X/N90s*, F90-series/N90*, F/N80-series*, F/N75-series*, F70-series/N70*, F/N65-series*, Pronea 600i/6i*, Pronea S	AF	Autofocus with manual override	Manual focus with electronic rangefinder
	MF	Manual focus (electronic rangefinder available with all cameras except F-601M/N6000*)	
F60-series/N60*, F/N55-series*, F50-series/N50*, F-801s/N8008s*, F-801/N8008*, F-601M/N6000*, F-401x/N5005*, F-401s/N4004s*, F-401/N4004*	AF, MF		

* N-series cameras and Pronea 6i sold in U. S. A. only.

M/A (Autofocus with Manual Override)

To focus using autofocus with manual override (M/A):

1 **Slide the lens focus-mode switch to M/A.**

2 **Focus.**
If desired, autofocus can be over-ridden by rotating the lens focus ring while the shutter-release button is pressed halfway (or, if the camera is equipped with an **AF-ON** button, while the **AF-ON** button is pressed). To refocus using autofocus, press the shutter-release button halfway or press the **AF-ON** button again.

■ Depth of Field

The depth-of-field indicators on the lens show the approximate depth of field (see page 172 for more information). If the camera offers depth-of-field preview (stop down), depth of field can also be previewed in the viewfinder.

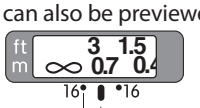

Depth-of-field indicators — *Focus distance mark*

■ Aperture

Aperture is adjusted using camera controls.

■ Built-in Flash Units

When using the built-in flash on cameras equipped with a built-in flash unit, shoot at ranges of 0.6 m (2 ft) or more and remove the lens hood to prevent vignetting (shadows created where the end of the lens obscures the built-in flash).

■ The Lens Hood

The lens hoods protect the lens and block stray light that would otherwise cause flare or ghosting.

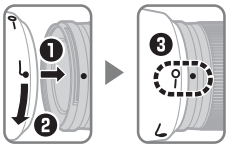

Align the lens hood lock mark (—○) with the lens hood mounting mark (●) on the lens (❸).

When attaching or removing the hood, hold it near the ⌐ symbol on its base and avoid gripping it too tightly. Vignetting may occur if the hood is not correctly attached.

The hood can be reversed and mounted on the lens when not in use. When the hood is reversed, it can be attached and removed by rotating it while holding it near the lock mark (—○).

■ Focusing Screens

The following cameras support a variety of focusing screens for use in different situations.

Camera \ Screen	A	B	C	E	EC-B EC-E	G1	G2	G3	G4	J	L	M	U
F6	◎	◎	—	◎	—	—	—	—	—	◎	◎		◎
F5+DP-30	◎	◎		◎	◎		◎			◎	◎		◎
F5+DA-30	◎	◎		◎	◎		◎ (+0.5)			◎	◎		◎

◎: Recommended.
○: Vignetting visible in viewfinder (photographs are not affected).
—: Not compatible with camera.
( ): Figures in parentheses give the exposure compensation for center-weighted metering. Select "Other screen" for Custom Setting b6 ("Screen comp.") when adjusting exposure compensation for the F6; note that with screens other than B or E, "Other screen" must be selected even when the value for exposure compensation is 0. Exposure compensation for the F5 can be adjusted using Custom Setting 18; see the camera manual for details.
Empty cell: Not suited to use with this lens. Note that type M screens can however be used for photomicrography and macro photography at magnifications of 1 : 1 or higher.

Note: The F5 supports matrix metering with A, B, E, EC-B/EC-E, J, and L focusing screens only.

■ Lens Care

- Do not pick up or hold the lens or camera using only the lens hood.
- Keep the CPU contacts clean.
- Should the rubber lens-mount gasket be damaged, cease use immediately and take the lens to a Nikon-authorized service center for repair.
- Use a blower to remove dust and lint from the lens surfaces. To remove smudges and fingerprints, apply a small amount of ethanol or lens cleaner to a soft, clean cotton cloth or lens-cleaning tissue and clean from the center outwards using a circular motion, taking care not to leave smears or touch the glass with your fingers.
- Never use organic solvents such as paint thinner or benzene to clean the lens.
- The lens hood or NC filters can be used to protect the front lens element.
- Attach the front and rear caps before placing the lens in its flexible pouch.
- If the lens will not be used for an extended period, store it in a cool, dry location to prevent mold and rust. Do not store in direct sunlight or with naphtha or camphor moth balls.
- Keep the lens dry. Rusting of the internal mechanism can cause irreparable damage.
- Leaving the lens in extremely hot locations could damage or warp parts made from reinforced plastic.

■ Supplied Accessories

- 67 mm snap-on Front Lens Cap LC-67
- Rear Lens Cap LF-4
- Bayonet Hood HB-64
- Flexible Lens Pouch CL-0915

■ Compatible Accessories

- 67 mm screw-on filters
- **Wireless Remote Speedlight SB-R200**: Up to two SB-R200 wireless remote flash units can be mounted at the end of the lens.

■ Specifications

Type	Type G AF-S lens with built-in CPU and F mount
Focal length	28 mm
Maximum aperture	f/1.8
Lens construction	11 elements in 9 groups (including 2 aspherical lens elements, and lens elements with Nano-Crystal coatings)
Angle of view	• **Nikon film SLR and FX-format D-SLR cameras**: 75° • **Nikon DX-format D-SLR cameras**: 53° • **IX240 system cameras**: 63°
Distance information	Output to camera
Focusing	**R**ear **F**ocusing (RF) System with autofocus controlled by Silent Wave Motor and separate focus ring for manual focus
Focus distance indicator	0.25 m to infinity (∞)
Minimum focus distance	0.25 m (0.82 ft) from focal plane
Diaphragm blades	7 (rounded diaphragm opening)
Diaphragm	Fully automatic
Aperture range	f/1.8 to f/16
Metering	Full aperture
Filter-attachment size	67 mm (P = 0.75 mm)
Dimensions	Approx. 73 mm maximum diameter × 80.5 mm (distance from camera lens mount flange)
Weight	Approx. 330 g (11.6 oz)

Nikon reserves the right to change the specifications of the hardware described in this manual at any time and without prior notice.

B.3. Fluke Ti32 IR camera

TECHNICAL DATA

Fluke Ti32 Thermal Imagers

Key features

- Delivers the clear, crisp images needed to find problems fast with its 320x240 sensor.
- Identify even the smallest temperature differences that could indicate problems with industry-leading thermal sensitivity (NETD).
- Automatic alignment (parallax correction) of visual and infrared images with Fluke patented IR-Fusion®
- Optional telephoto and wide angle lenses available for added versatility and special applications. (easily installable in the field)

Easy to use

- Field replaceable batteries give you maximum flexibility no matter where your work takes you.
- Intuitive, three-button menu is easy to use—simply navigate with the push of a thumb.
- No need to carry pen and paper—record findings by speaking into the imager. Voice annotations can be recorded with every image you take. Voice comments are saved along with individual images for future reference.
- One-handed focus capability, emissivity correction, reflected background temperature compensation, and transmission correction increase the accuracy of measurements in most situations.
- Adjustable hand strap for left-or right-handed use.
- Everything needed to get started is included.

Rugged

- Optimized for field use in challenging work environments.
- Engineered and tested to withstand a 2 m drop for the ultimate peace of mind - When was the last time you dropped a tool or piece of equipment?
- Withstands dust and water—tested to an IP54 rating.

Product overview: Fluke Ti32 Thermal Imagers

Top of the range High Definition Thermal Imager, that's truly affordable.

Built for top professionals, the Ti32 is a tool you can use everywhere, from troubleshooting actual defects to spotting potential failures during regular service and maintenance. With its superior image quality, optional lenses, field-swappable batteries and intuitive user interface, the rugged Ti32, a superior infrared camera is ideal for busy, front line engineers who are always on the go

Specifications: Fluke Ti32 Thermal Imagers

Temperature		
Temperature measurement range (not calibrated below -10°C)	-20°C to +600°C (-4°F to +1112°F)	
Temperature measurement accuracy	±2°C or 2% (at 25°C nominal, whichever is greater)	
On-screen emissivity correction	Yes	
On-screen reflected background temperature compensation	Yes	
On-screen transmission correction	Yes	
Imaging Performance		
Image capture frequency	9 Hz refresh rate or 60 Hz refresh rate depending upon model variation	
Detector type	320 X 240 Focal Plane Array, uncooled microbolometer	
Thermal sensitivity (NETD)	≤ 0.045 degrees C and 45 mK	
Total pixels	76,800	
Infrared spectral band	7.5 µm to 14 µm (long wave)	
Visual (visible light) camera	Industrial performance 2.0 megapixel	
Minimum focus distance	46 cm (approx. 18 in)	
Standard infrared lens type	**Field of view**	23° x 17°
	Spatial resolution (IFOV)	1.25 mRad
	Minimum focus distance	15 cm (approx. 6 in)
Optional telephoto infrared lens type	**Field of view**	11.5° x 8.7°
	Spatial resolution (IFOV)	0.63 mRad
	Minimum focus distance	45 cm (approx. 18 in)
Optional wide-angle infrared lens type	**Field of view**	46° x 34
	Spatial resolution (IFOV)	2.50 mRad
	Minimum focus distance	7.5 cm (approx. 3 in)
Focus mechanism	Manual, one-handed Smart Focus capability	
Image Presentation		

Palettes	**Standard**	Ironbow, blue-red, high contrast, amber, amber inverted, hot metal, grayscale, grayscale inverted
	Ultra Contrast™	Ironbow ultra, blue-red ultra, high contrast ultra, amber ultra, amber inverted ultra, hot metal ultra, grayscale ultra, grayscale inverted
Level and span	Smooth auto-scaling and manual scaling of level and span	
Fast auto toggle between manual and auto modes	Yes	
Fast auto-rescale in manual mode	Yes	
Minimum span (in manual mode)	2.5°C (4.5°F)	
Minimum span (in auto mode)	5°C (9°F)	
IR-Fusion® Information		
Automatically aligned (parallax corrected) visual and IR blending	Yes	
Picture-in-picture (PIP)	Three levels of on-screen IR blending displayed in center of LCD	
Full screen infrared	Three levels of on-screen IR blending displayed in center of LCD	
Color alarms (temperature alarms)	High-temperature alarm (user-selectable)	
Image Capture and Data Storage		
Image capture, review, save mechanism	The Ti32 allows user to adjust palette, blending, level, span, IR-Fusion® mode, emissivity, and reflected background temperature compensation, and transmission correction on a captured image before it is stored.	
Voice annotation	60 seconds maximum recording time per image; reviewable playback on imager	
Storage medium	One-handed image capture, review, and save capability	
File formats	SD Memory Card (2 GB memory card will store at least 1200 fully radiometric (.is2) IR and linked visual images each with 60 seconds voice annotations, or 3000 basic bitmap (.bmp) images, or 3000 jpeg (.jpeg) images; transferrable to PC via included multi-format USB card reader	
Export file formats w/SmartView® software	Non-radiometric (.bmp) or (.jpeg) or fully-radiometric (.is2) No analysis software required for non-radiometric (.bmp and .jpeg) files	
General Specifications		
Operating temperature	-10°C to +50°C (14°F to 122°F)	
Storage temperature	-20°C to +50°C (-4°F to 122°F) without batteries	
Relative humidity	10% to 95% non-condensing	
Display	9.1 cm (3.7 in) diagonal landscape color VGA (640 x 480) LCD with backlight and clear protective cover	

Controls and adjustments	User selectable temperature scale (°C/°F) Language selection Time/Date set Emissivity selection Reflected background temperature compensation Transmission correction User selectable hot spot and cold spot, and center point on the image (other custom markers and shapes in SmartView® software) High temperature alarm User selectable backlight: "Full Bright" or "Auto" Information display preference
Software	SmartView® full analysis and reporting software included
Batteries	Two lithium ion rechargeable smart battery packs with five-segment LED display to show charge level
Battery life	Four+ hours continuous use per battery pack (assumes 50% brightness of LCD)
Battery charge time	2.5 hours to full charge
AC battery charging	Two-bay AC battery charger (110 V AC to 220 V AC, 50/60 Hz) (included), or in-imager charging. AC mains adapters included. Optional 12 V automotive charging adapter.
AC operation	AC operation with included power supply (110 V AC to 220 V AC, 50/60 Hz). AC mains adapters included.
Power saving	Sleep mode activated after five minutes of inactivity, automatic power off after 30 minutes of inactivity
Safety standards	CSA (US and CAN): C22.2 No. 61010-1-04, UL: UL STD 61010-1 (2nd Edition), ISA: 82.02.01
Electromagnetic compatibility	Meets all applicable requirements in EN61326-1:2006
C Tick	IEC/EN 61326-1
US FCC	CFR 47, Part 15 Class B
Vibration	0.03 g^2/Hz (3.8 grms), IEC 68-2-6
Shock	25 g, IEC 68-2-29
Drop	2 m (6.5 ft) with standard lens
Dimensions (H x W x L)	27.7 x 12.2 x 17.0 cm (10.9 x 4.8 x 6.7 in)
Weight (battery included)	1.05 kg (2.3 lb)
Enclosure rating	IP54 (protected against dust, limited ingress; protection against water spray from all directions)
Warranty	Two-years (standard)
Recommended calibration cycle	Two-years (assumes normal operation and normal aging)
Supported languages	Czech, English, Finnish, French, German, Italian, Japanese, Korean, Polish, Portuguese, Russian, Simplified Chinese, Spanish, Swedish, Traditional Chinese, and Turkish

B.4. Fluke 568 IR thermometer

Fluke 566 and 568 Thermometers

Technical Data

Two-in-one infrared and contact thermometers with an innovative dot matrix display.

Just when you thought advanced IR temperature measurement should be easier! With a straight-forward user interface and soft-key menus, the Fluke 566 and 568 make even complex measurements easy. Quickly navigate and adjust emissivity, start data logging, or turn on and off alarms, with just a few pushes of a button.

With a rugged, easy-to-use, ergonomic design, the Fluke 566 and 568 can stand up to tough industrial, electrical, and mechanical environments.

- Measure –40 °C to 800 °C /–40 °F to 1472 °F (568) or –40 °C to 650 °C/–40 °F to 1202 °F (566)
- Easily access advanced features with the soft-key buttons and graphical display
- Measure smaller objects from further away, with a distance-to-spot ratio of 50:1 (568) or 30:1 (566)
- Compatibility with all standard miniconnector K-type thermocouples allows you to preserve your thermocouple investments
- Confidently measure a wide variety of surfaces with the adjustable emissivity feature, including a built-in material table
- Capture up to 99 points (568) or 20 point (566) of data, for downloading and recalling later
- Easily trend and analyze data with included FlukeView® Forms software (568)
- See your data right away without leaving the site, using the USB (568) and your laptop for "Hands-free" datalogging
- Confidently troubleshoot equipment with 1 % measurement accuracy
- Versatile interface with six languages from which to choose
- Two-year warranty

Product specifications

	566	568
Infrared temperature range	–40 °C to 650 °C (–40 °F to 1202 °F)	–40 °C to 800 °C (–40 °F to 1472 °F)
Infrared accuracy	< 0 °C (32 °F): ± (1.0 °C (± 2.0 °F) + 0.1°/1 °C or °F); > 0 °C (32 °F): ± 1 % or ± 1.0 °C (± 2.0 °F), whichever is greater	
Display resolution	0.1 °C / 0.1 °F	
Infrared spectral response	8 µm to 14 µm	
Infrared response time	< 500 msec	
Thermocouple Type-K input temperature range	–270 °C to 1372 °C (–454 °F to 2501 °F)	
Thermocouple Type-K input accuracy	–270 °C to –40 °C: ± (1 °C + 0.2 °/1 °C) (–454 °F to –40 °F: ± (2 °F + 0.2 °/1 °F)) –40 °C to 1372 °C: ± 1 % or 1 °C (–40 °F to 2501 °F: ± 1 % or 2 °F), whichever is greater	
D:S (distance to measurement spot size)	30:1	50:1
Laser sighting	Single-point laser < 1 mw output Class 2 (II) operation, 630 nm to 670 nm	
Minimum spot size	19 mm (0.75 in)	
Emissivity adjustment	By built-in table of common materials or digitally adjustable from 0.10 to 1.00 by 0.01	
Data storage with Date/Time stamp	20 points	99 points
PC Interface and cable	None	USB 2.0 with FlukeView® Forms software
Hi/Low alarms	Audible and two-color visual	
Min/Max/Avg/Dif	Yes	
Display	Dot matrix 98 x 96 pixels with function menus	
Backlight	Two levels, normal and extra bright for darker environments	
Trigger lock	Yes	
Switchable Celsius and Fahrenheit	Yes	
Power	2 AA/LR6 Batteries	2 AA/LR6 Batteries and USB when used with a PC
Battery life	If used continuously: laser and backlight on,12 hours; laser and backlight off, 100 hours	
Operating temperature	0 °C to 50 °C (32 °F to 122 °F)	
Storage temperature	–20 °C to 60 °C (–40 °F to 140 °F)	
Bead thermocouple Type-K range	–40 °C to 260 °C (–40 °F to 500 °F)	
Bead thermocouple Type-K accuracy	± 1.1 °C (2.0 °F) from 0 °C to 260 °C (32 °F to 500 °F), typically within 1.1 °C (2.0 °F) from –40 °C to 0 °C (–40 °F to 32 °F)	

Ordering information

Fluke-566 Infrared thermometer
Fluke-568 Infrared thermometer

Includes: Infrared thermometer with contact thermometer capabilities, FlukeView® Forms software (568 only), USB cable (568 only), K-type thermocouple bead probe, hard carrying case, quick start guide, and users manual.

Fluke. *Keeping your world up and running.®*

Fluke Corporation
PO Box 9090, Everett, WA 98206 U.S.A.

Fluke Europe B.V.
PO Box 1186, 5602 BD
Eindhoven, The Netherlands

For more information call:
In the U.S.A. (800) 443-5853 or
Fax (425) 446-5116
In Europe/M-East/Africa +31 (0) 40 2675 200 or
Fax +31 (0) 40 2675 222
In Canada (800)-36-FLUKE or
Fax (905) 890-6866
From other countries +1 (425) 446-5500 or
Fax +1 (425) 446-5116
Web access: http://www.fluke.com

Printed in U.S.A. 8/2007 3085001 D-EN-N Rev A